Bulletin of the Seismological Society of America, Vol. 94, No. 6B, pp. S107–S131, December 2004

Geophysical Data Reveal the Crustal Structure of the Alaska Range Orogen within the Aftershock Zone of the M_w 7.9 Denali Fault Earthquake

by Michael A. Fisher, Natalia A. Ratchkovski, Warren J. Nokleberg, Louise Pellerin, and Jonathan M. G. Glen

Abstract Geophysical information, including deep-crustal seismic reflection, magnetotelluric (MT), gravity, and magnetic data, cross the aftershock zone of the 3 November 2002 M_w 7.9 Denali fault earthquake. These data and aftershock seismicity, jointly interpreted, reveal the crustal structure of the right-lateral-slip Denali fault and the eastern Alaska Range orogen, as well as the relationship between this structure and seismicity. North of the Denali fault, strong seismic reflections from within the Alaska Range orogen show features that dip as steeply as 25° north and extend downward to depths between 20 and 25 km. These reflections reveal crustal structures, probably ductile shear zones, that most likely formed during the Late Cretaceous, but these structures appear to be inactive, having produced little seismicity during the past 20 years. Furthermore, seismic reflections mainly dip north, whereas alignments in aftershock hypocenters dip south. The Denali fault is nonreflective, but modeling of MT, gravity, and magnetic data suggests that the Denali fault dips steeply to vertically. However, in an alternative structural model, the Denali fault is defined by one of the reflection bands that dips to the north and flattens into the middle crust of the Alaska Range orogen. Modeling of MT data indicates a rock body, having low electrical resistivity (>10 Ω·m), that lies mainly at depths greater than 10 km, directly beneath aftershocks of the Denali fault earthquake. The maximum depth of aftershocks along the Denali fault is 10 km. This shallow depth may arise from a higher-than-normal geothermal gradient. Alternatively, the low electrical resistivity of deep rocks along the Denali fault may be associated with fluids that have weakened the lower crust and helped determine the depth extent of the aftershock zone.

Introduction

On 3 November 2002, seismic activity in south-central Alaska culminated in an M_w 7.9 earthquake that ruptured along the Denali fault (Fig. 1). This activity eventually generated a complicated earthquake sequence that ruptured along the Denali and other faults for a total distance of nearly 340 km (Eberhart-Phillips *et al.*, 2003). The right-lateral, strike-slip Denali fault is a major tectonic element of the Alaska Range orogen of south-central Alaska. The fault extends generally westward for about 1500 km from western Canada to near the shore of the Bering Sea (Grantz, 1966; Brogan *et al.*, 1975; Wahrhaftig *et al.*, 1975). Geologists have long scrutinized the Denali fault because it poses a significant seismic hazard; moreover, the fault is thought to have played a prominent role in the northward translation and amalgamation of Alaskan tectonostratigraphic terranes (Csejtey *et al.*, 1982; Plafker *et al.*, 1989; Nokleberg *et al.*, 1994; Ridgway *et al.*, 2002). According to one tectonic model (Nokleberg *et al.*, 1994), during the Cretaceous, rocks making up much of the Alaska Range orogen lay along the southern continental margin of Alaska, and oblique-convergent motion along the ancestral Denali fault resulted in the collision and suturing of numerous terranes against Alaska. During the Early Cenozoic, the right-lateral strike-slip Denali fault developed within this collision and suture zone, and since then motion along this fault has facilitated the westward tectonic escape of rocks lying along the fault's south side. Thus, the M_w 7.9 Denali fault earthquake ruptured along a fault system that has had an enduring and complicated evolution.

We investigate the crustal structure of the Denali fault and Alaska Range orogen, using outcrop geology, earthquake distribution, and a diverse suite of geophysical information. This suite includes deep-crustal seismic reflection, magnetotelluric (MT), gravity, and magnetic data. Geophysical data discussed herein form a transect along the Richardson Highway, which winds through the mountainous terrain

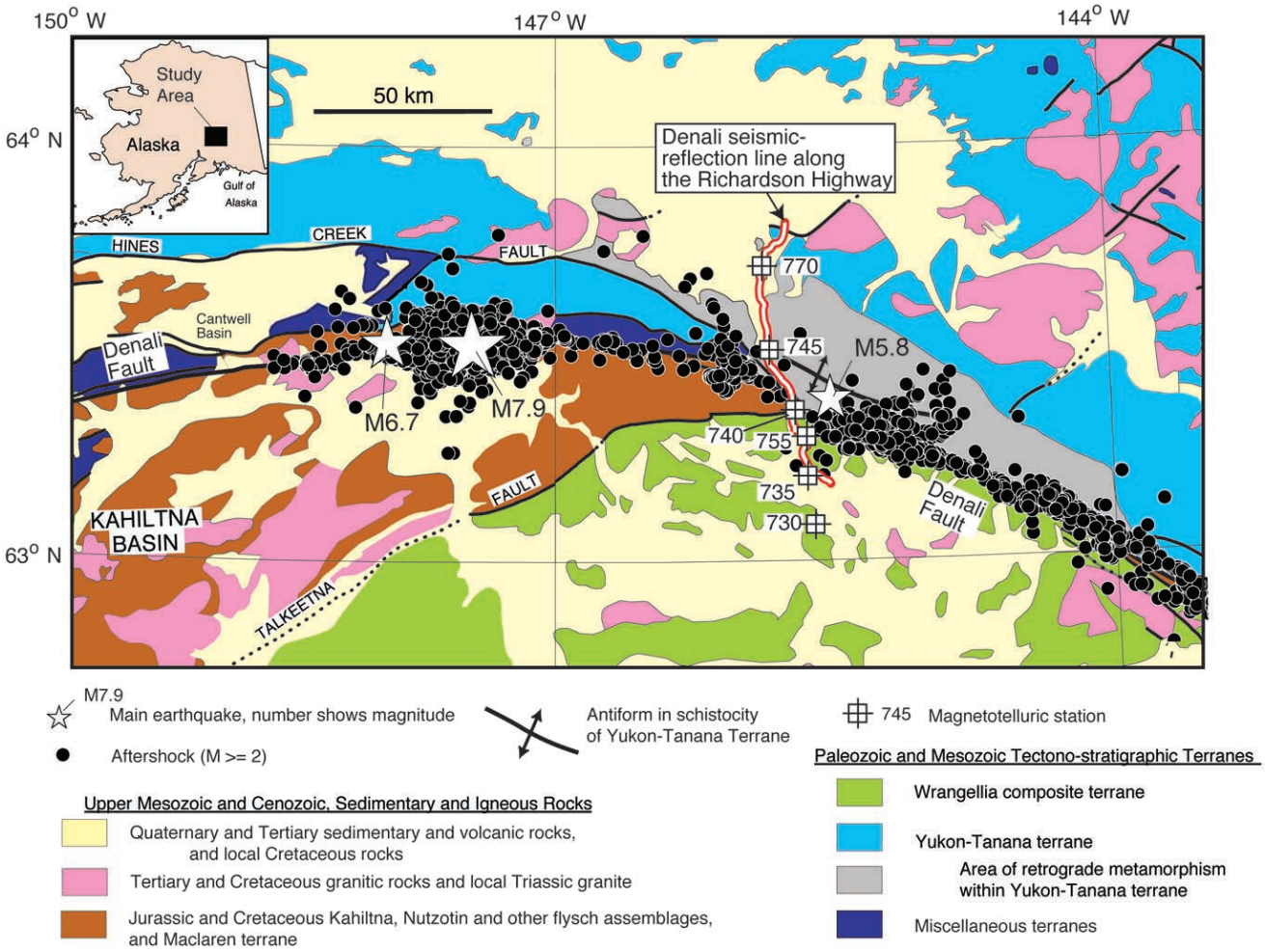

Figure 1. Geology of the study area and seismicity associated with the Denali fault earthquake. Geology simplified from Ridgway *et al.* (2002). Geophysical data shown herein were collected along the Richardson Highway, about 100 km east of the epicenter of the Denali fault earthquake.

of the Alaska Range and crosses the regional geologic strike at a high angle (Fig. 1). The geophysical transect and the Denali fault intersect within the aftershock zone of the Denali fault earthquake, about 100 km east of the mainshock. Intriguing findings from geophysical data include: (1) rocks having low electrical resistivity underlie the aftershock zone and the surface trace of the Denali fault, and (2) seismic reflection data show strong, north-dipping reflections from depths as great as 25 km within the Alaska Range orogen. We investigate the relationships among crustal structure, seismicity, and features revealed by geophysical data.

The 2002 Earthquake Sequence

The M_w 6.7 Nenana Mountain earthquake preceded the Denali fault earthquake by 11 days (Eberhart-Phillips *et al.*, 2003); the foreshock was located about 20 km west of the mainshock (Fig. 1). The Denali fault earthquake sequence involved three large subevents (Eberhart-Phillips *et al.*, 2003; Dreger *et al.*, 2004). The second subevent has particular importance for this report in that the event originated west of where the Denali fault and the Richardson Highway intersect, and fault rupture then propagated eastward across the highway to the far eastern limit of the rupture zone. The Denali fault earthquake generated thousands of aftershocks (Ratchkovski *et al.*, 2003). The largest aftershock (M_L 5.8) occurred about 10 km east of the Richardson Highway and the geophysical transect described herein (Fig. 2).

To correlate regional seismicity with the aftershock locations, we used the double-difference algorithm (Waldhauser and Ellsworth, 2000) to relocate jointly the 2002 sequence aftershocks and the sparse regional seismicity that occurred between 1975 and the 2002 Denali fault earthquake. We selected only events with $M_L \geq 2$ for the relocation. The horizontal and vertical location uncertainties for the regional and aftershock events are 1.87 and 3.10 km and 0.40 and 0.89 km, respectively. Use of the temporary stations located near the ruptured Denali fault greatly reduced

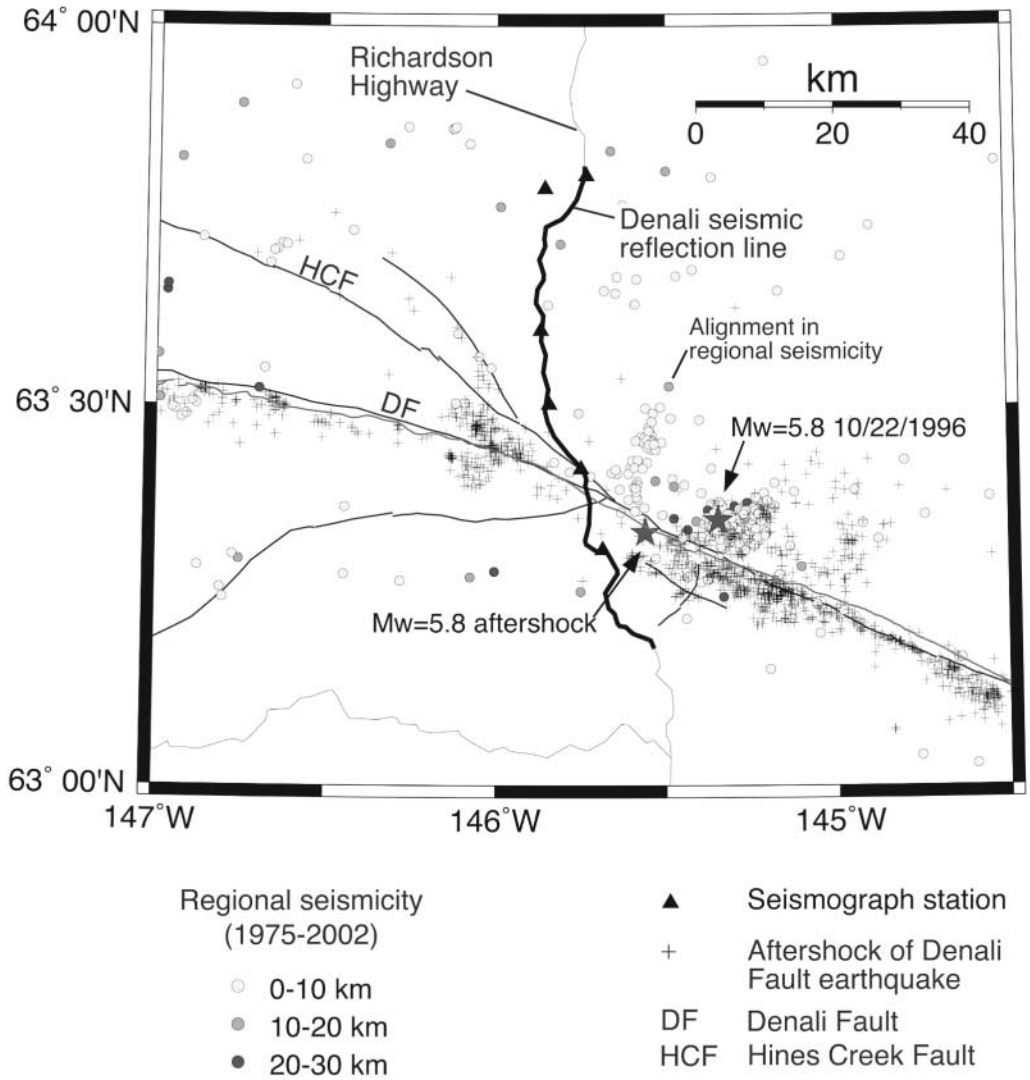

Figure 2. Historical seismicity along the Denali fault near the geophysical transect.

location uncertainties of the aftershocks (Ratchkovski *et al.*, 2003). The relative location errors after the double-difference relocation are within 0.5 km.

The relocation results show that the majority of aftershocks are shallow, clustering within the upper 10 km of the crust (see cross sections in Fig. 3). The most notable recent regional earthquake prior to the 2002 earthquake sequence was the M_w 5.8 event (22 October 1996) located north of the Denali fault trace and about 20 km east of the Richardson Highway crossing (Fig. 2). Like the 2002 aftershocks, the earlier regional seismicity near the Denali fault trace was concentrated mainly within the upper 10 km of the crust.

Comparison of the regional and aftershock seismicity (Fig. 2) reveals few substantive differences in their geographic distributions. For example, the area around the 1996 M_w 5.8 event was seismically active before 2002, and an aftershock cluster occurred in the same area. Furthermore, the largest aftershock struck within 10 km of the earlier M_w 5.8 event. The main difference between regional and aftershock events appears to be the northeast-trending alignment of regional seismicity (Fig. 2), located about 10 km east of the Richardson Highway, that had few coincident aftershocks.

Three hypocenter cross sections reveal the varied distribution of the aftershock seismicity from west to east along the Denali fault (Fig. 3). The Hines Creek and Denali faults converge near the Richardson Highway, as discussed below (Fig. 1; index map in Fig. 2), and the aftershock hypocenters (section D) provide few coherent details about the internal structure of what undoubtedly is a complexly structured zone within the Alaska Range orogen. In contrast, east of the Richardson Highway (section E), hypocenters south of the Denali fault dip north and appear to end downward at about 7 km depth, below the fault's surface trace. Farther east of the highway (section F), another hypocentral alignment begins at shallow depths north of the Denali fault and dips south to where it, too, ends at about 7 km below the Denali fault's surface trace. One consistent feature of the hypocen-

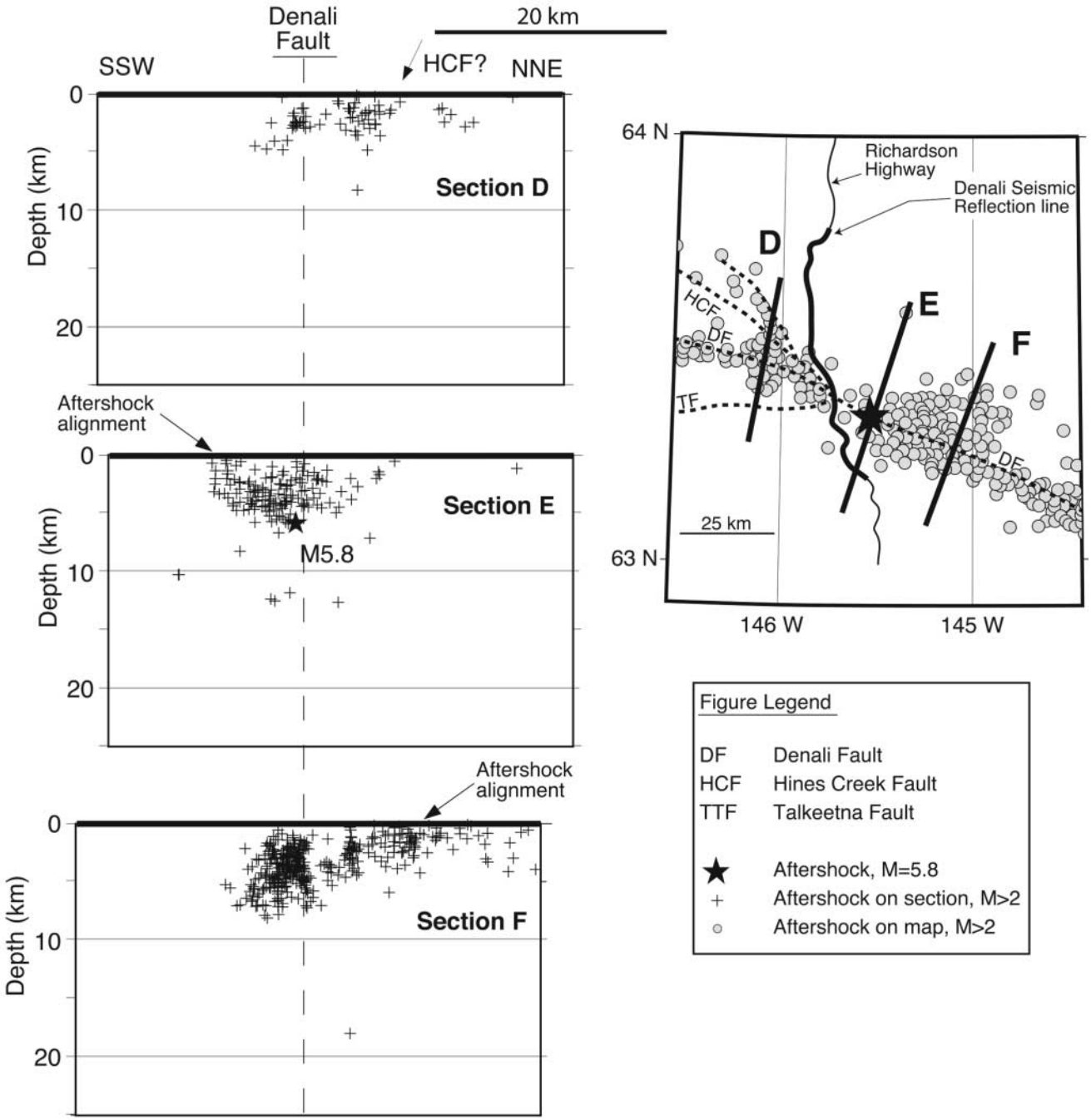

Figure 3. Three hypocenter cross sections, perpendicular to the Denali fault, showing the distribution of aftershocks from the Denali fault earthquake in the area of the geophysical transect (modified from data in Ratchkovski *et al.*, 2003). Hypocenters within 10 km of the cross sections were projected parallel to the Denali fault onto the sections.

tral distribution is that hypocenters deepen eastward from section D to section F. The main finding, however, is that west to east through the narrow swath across the Denali fault that is illustrated in Figure 3, hypocenters suggest some variation in the attitude of seismogenic structures. Because the relative and absolute location uncertainties of the aftershocks are less than 1 km, we are convinced that these variations are real. This complexity is mirrored in the strong along-strike variation in the geology of the Alaska Range, as we discuss next.

Geologic Setting

The Alaska Range orogen near the Richardson Highway includes numerous tectonostratigraphic terranes and major fault zones (e.g., Nokleberg *et al.*, 1994; Ridgway *et al.*,

2002), many of which converge near the intersection between the geophysical transect and the Denali fault (Figs. 1 and 4). We discuss these terranes and the main faults from south to north.

Terranes South of the Denali Fault

The extensive Wrangellia terrane lies south of the Denali fault (Figs. 1 and 4). The oldest units of this terrane are upper Paleozoic volcanic and sedimentary rocks (Plafker *et al.*, 1989; Panuska, 1990; Nokleberg *et al.*, 1994; Ridgway *et al.*, 2002; Trop *et al.*, 2002). These rocks are disconformably overlain by (1) Upper Triassic basalt (the Nikolai Greenstone; Nokleberg *et al.*, 1985, 1994) and limestone; (2) an overlap assemblage of Upper Jurassic and Lower Cretaceous island-arc volcanic rocks and flysch; and (3) a sequence of Tertiary continental sedimentary and volcanic rocks (Bond, 1973, 1976; Nokleberg *et al.*, 1982, 1985). Paleomagnetic data indicate that this terrane formed within about 14° of the Triassic equator (Hillhouse and Gromme, 1984; Sontag and Panuska, 1990; Stone *et al.*, 1991). The Nikolai Greenstone includes mafic and ultramafic intrusives that produce strong magnetic anomalies.

The Kahiltna, Maclaren, and Windy terranes and other closely associated rocks, included in units shown in brown on Figure 1, consist of a Jurassic and Cretaceous sequence of sedimentary and volcanic rocks and their variably metamorphosed equivalents as well as regionally metamorphosed and deformed granitic rocks (Nokleberg *et al.*, 1982, 1985). The metamorphic protolith of the Maclaren terrane is interpreted to be flysch similar to rocks that make up the Kahiltna terrane (Richter, 1976; Smith, 1981; Stout, 1976). This terrane includes extensively exposed Upper Jurassic and Lower Cretaceous flysch that is interpreted to be a remnant of a Jurassic and Cretaceous basin that originally extended for several thousand kilometers along the margin of the North American Cordillera. These flysch deposits constitute one of the major stratigraphic units in southern and southeastern Alaska, despite their dismemberment and wide dispersal along major faults (Richter and Jones, 1973; Richter, 1976; Monger and Berg, 1987; Wallace *et al.*, 1989; Rubin and Saleeby, 1991; Ridgway *et al.*, 2002).

The Denali and Hines Creek Faults

Numerous major thrust and strike-slip faults cleave the eastern Alaska Range; chief among them is the right-lateral, strike-slip Denali fault. Nokleberg *et al.* (1994) summarize evidence for substantial late Mesozoic and early Cenozoic dextral displacement along the Denali fault. During the Cretaceous, oblique-slip underthrusting may have occurred along the ancestral Denali fault, as interpreted partly from the history of metamorphism of rocks that make up the Yukon-Tanana terrane along the fault's north side (Nokleberg *et al.*, 1994; Ridgway *et al.*, 2002). Estimates of Quaternary movement on the Denali fault range from 1 to 6.5 km since early Wisconsin or Illinoisan time (Richter and Matson, 1971; Stout *et al.*, 1973). Probable rates of Holocene movement average 1.5 cm per year (Plafker *et al.*, 1994). Recent Global Positioning System (GPS) measurements indicate 6 to 8 mm/yr of right-lateral strike-slip motion across the Alaska Range (Freymueller *et al.*, 2003).

The Hines Creek fault is a zone of intense shearing and penetrative deformation that extends more than 100 km westward from where it branches to the north away from the Denali fault, near the Richardson Highway (Wahrhaftig *et al.*, 1975) (Figs. 1 and 4). This fault has a history of complex strike-slip and thrust movement that spanned from the Middle Cretaceous into the Cenozoic.

Terranes North of the Denali Fault

The Aurora Peak terrane (Aleinikoff, 1984; Nokleberg *et al.*, 1985) (Fig. 4) consists of probable Paleozoic or early Mesozoic sedimentary rocks that were metamorphosed to calcschist, marble, quartzite, and pelitic schist. Late Cretaceous and early Tertiary plutonic rocks that intruded into this terrane are regionally metamorphosed and penetratively deformed (Nokleberg *et al.*, 1985; W. J. Nokleberg and J. N. Aleinikoff, unpublished data, 1984).

Multiply deformed and metamorphosed rocks of the Yukon-Tanana terrane (YTT) underlie most of the Denali seismic reflection line and many of the field stations for the other types of geophysical data (Figs. 1 and 4). This extensively exposed terrane spans the region between the Denali fault on the south and the Tintina fault on the north—a distance of about 250 km (Nokleberg *et al.*, 1989; Dusel-Bacon, 1991; McClelland *et al.*, 1992; Ridgway *et al.*, 2002). Isotopic data indicate that metamorphism of the YTT occurred during the Early Jurassic and again during the Middle to Late Cretaceous (115 to 102 Ma) (Turner and Smith, 1974; Aleinikoff and Nokleberg, 1985; Nokleberg *et al.*, 1986; Aleinikoff *et al.*, 1986). These metamorphic episodes affected Devonian and older sedimentary and subordinate volcanic rocks. Exposed at the deepest known structural level of the YTT are high-grade schists, gneiss, and augen gneiss that have middle Cretaceous cooling ages. During Late Cretaceous (~105 Ma) retrograde metamorphism of the YTT, a major antiform developed that follows the north side of the Denali and Hines Creek faults for more than 50 km (axis shown in Figs. 1 and 4). This fold deforms the metamorphic schistosity, which is flat except in the fold where it locally steepens to nearly vertical. This fault-parallel antiform figures prominently in the interpretation of seismic reflection data.

Cenozoic Rocks and Structures

The thickest Cenozoic rocks near the geophysical transect comprise the Paleocene fill of the Cantwell basin (Hickman *et al.*, 1991), which lies about 150 km west of where the Richardson Highway and the geophysical transect cross

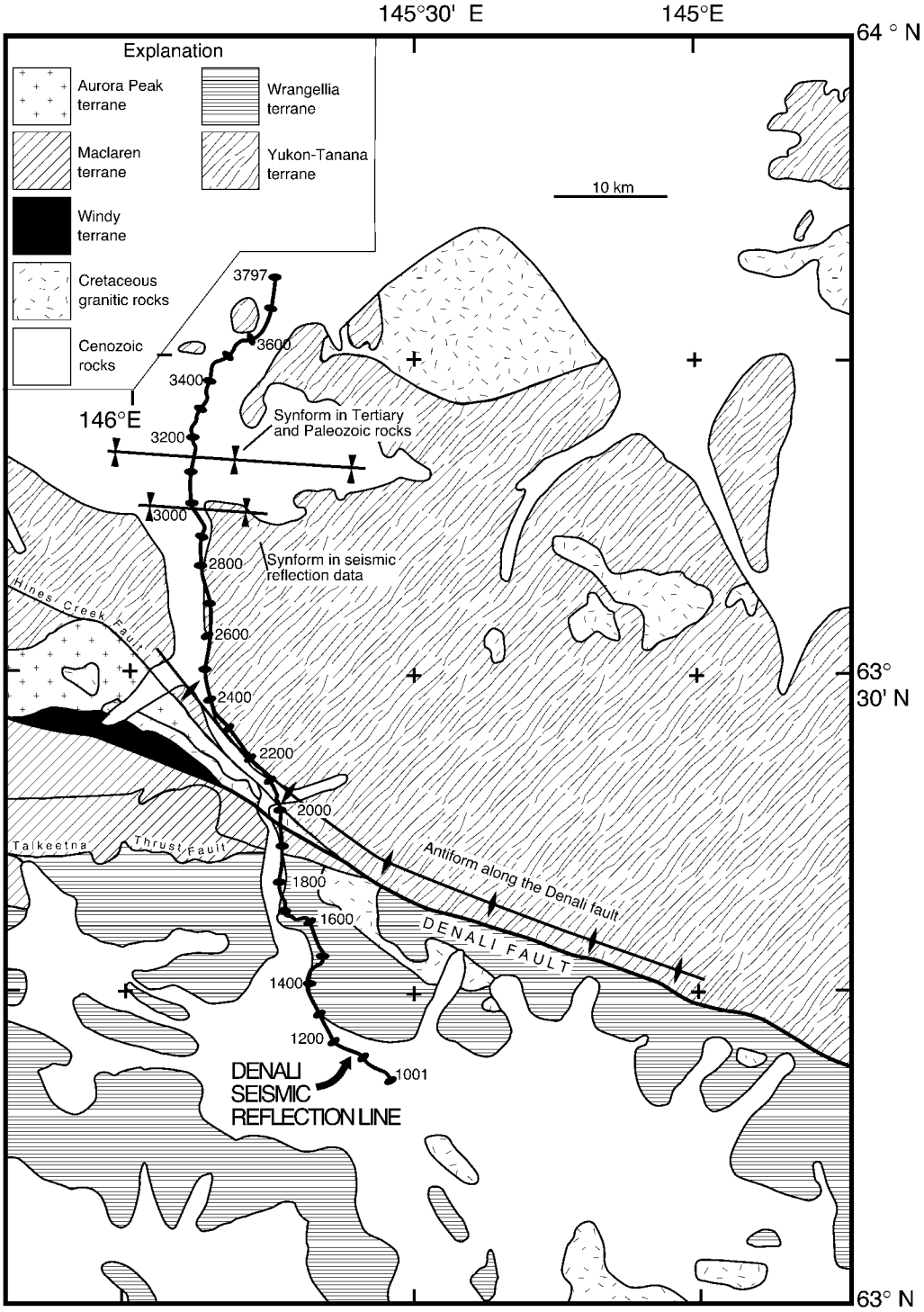

Figure 4. Detailed geology and vibrator-point (VP) locations for the Denali seismic reflection line.

the Denali fault (Fig. 1). This basin is bounded by the Hines Creek fault on the north and the Denali fault on the south, and the basin fill provides some of the best information about the Cenozoic development of the Denali fault. During the Paleocene, normal dip slip occurred along the Denali fault, the basin subsided rapidly as an asymmetric half-graben, and a maximum of about 4000 m of sedimentary and volcanic rocks accumulated. During the Early Eocene the basin fill was strongly compressed when strike-slip offset began along the Denali fault.

The Denali seismic reflection line crosses thin accumulations of early Cenozoic sedimentary rocks. These rocks

fill a broad syncline that strikes east–west; the synclinal axis lies about 20 km north of the Denali fault (Fig. 4). The syncline is expressed not only in the early Cenozoic rocks but also in the concordantly folded schistosity of underlying metamorphic rocks.

Geophysical Information

Selected Results from Previous Geophysical Investigations

Synthetic-aperture radar interferometry (InSAR) data have been modeled to derive the fault movement that likely caused surface deformation associated with the Nenana Mountain (M_w 6.7 on Fig. 1) and Denali fault earthquakes (Lu *et al.*, 2003; Wright *et al.*, 2003). One result of this modeling is the Denali fault is estimated to dip 81°, at a location about 100 km west of the geophysical transect (Wright *et al.*, 2003). This is close in value to the dip (86°) determined from analysis of teleseismic arrivals (Kikuchi and Yamanaka, 2002). For the Denali fault earthquake, deformation along the section of the Denali fault that lies below and east of the geophysical transect is not well constrained by InSAR data, but the fault was assumed to be vertical during analysis of these data, to accord with findings about this fault farther west (Lu *et al.*, 2003). The Denali fault was also assumed to be vertical during modeling of GPS data (Hreinsdóttir *et al.*, 2003), on the basis of findings from teleseismic body waves (Kikuchi and Yamanaka, 2002). Other GPS modeling proceeded on the basis of a vertical Denali fault because hypocenters do not clearly delineate a nonvertical dip (Dreger *et al.*, 2004).

Brocher *et al.* (1991) estimated that the Moho depth below the Alaska Range along the Richardson Highway is about 50 km. This depth is similar to the depth range for the Moho derived from broadband receiver functions obtained along the Parks Highway, about 150 km west of the Richardson Highway; here, the Moho below the central part of the Alaska Range ranges from 38 to 46 km in depth (E. Veenstra, written comm., 2004).

Detailed rock-velocity information is not available from along the geophysical transect because of a poor signal-to-noise ratio in wide-angle seismic data (Brocher *et al.*, 1991). However, velocity data from 50 km north of the north end of the Denali seismic reflection line indicate that the crust making up the YTT, and hence much of the Alaska Range orogen, is thick (>30 km) and characterized throughout by low seismic *P*-wave velocities (~6.2 km/sec) (Beaudoin *et al.*, 1992; Plate 1,[1] right side of lower panel [unbound insert to this issue]).

[1] Plate 1: (Top) Migrated, depth-converted seismic reflection data from along the Denali seismic line. (Bottom) Assembled geophysical information over the Denali fault, including gravity and magnetic, seismic reflection, crustal-velocity, and magnetotelluric data, as well as seismicity. The plane of section used in making Plate 1 parallels the Richardson Highway, which is not perpendicular to the Denali fault (Figs. 1 and 3). Hypocenters shown on the plate lie within 10 km of the plane of section, measured along the strike of the Denali fault, and the hypocenters were projected parallel to this fault's strike onto the section.

Seismic Reflection Data

Collection and Processing of Seismic Reflection Data. Seismic reflection data were collected during the winter of 1986 for the U.S. Geological Survey and have a nominal 128 fold of coverage (Table 1). The data processing sequence (Table 2) that resulted in seismic sections shown in this report included migration after stack and conversion of time to depth, with a crustal velocity model (Brocher *et al.*, 1991) combined with stacking-velocity information. The Denali seismic reflection line followed the Richardson Highway (Fig. 4) and the resulting line orientation with respect to the regional geologic strike are not optimum for showing geologic structure, because north of vibrator point (VP) 2000 nearly to VP 2400 the seismic line maintains a constant standoff of about 3 km from the Hines Creek fault (Fig. 4). This parallelism increases the risk that out-of-plane events were recorded, complicating the seismic image of the crustal structure. North of VP 2400, the seismic line and the regional geologic strike diverge by about 70°, and strong reflections

Table 1
Field Parameters for the Acquisition of Seismic Reflection Data

Contractor	Geosystems Corporation
Recording instruments	GEOCOR IV, sign bit
Sample rate (m sec)	4
Corelated record length (sec)	24
Spread configuration	Symmetrical split, 15,360 m-0-15,360 m
Group interval (m)	30
Number of groups	1024
Nominal fold of converge	128
Vibrator point interval (m)	120
Source	5 Litton 311 vibrators
Total peak force (kg)	61,000
Sweep	Varisweep, 6 downsweeps repeated twice at each VP
Sweep length (sec)	20
Nominal source bandwidth (Hz)	10–30
Geophone pattern	6 geophones in a 2 m cluster

Table 2
Processing Sequence for the Migrated Section

Demultiplex
Datum statics (spatially variable replacement velocity)
Refraction statics
Bin common reflection points
Resample to 8 m sec
Prestack AGC (512 m sec operator)
Velocity analysis
Apply moveout
Mute
Residual statics
CDP stack
2:1 vertical stack
Migration
Time-variant filtering
Amplitude compensation

are evident from depths as great as 20 to 25 km (Plate 1, top).

Main Features in Seismic Reflection Data. Seismic reflection data collected south of the Denali fault reveal little about the structure of the igneous rocks that make up the Wrangellia terrane or the metasedimentary and plutonic rocks comprising the Kahiltna and Maclaren terranes (Plate 1, top). Shallow (<2 km) reflections, like those below VP 1050 and VP 1400, are probably from local accumulations of Cenozoic sedimentary rock, which have low seismic velocities (<4 km/sec) (Brocher *et al.*, 1991).

Signal strength decreases rapidly with increasing travel time in the poor-quality, seismic reflection data from the southern part of the Denali seismic line, explaining why no deep reflections are discernible there. The southern amplitudes decay much like the amplitude curve for VP 2200 (Fig. 5), which decays to ambient noise levels within the first 2 sec. In contrast, seismic reflection data from north of the Denali fault show high-amplitude events to travel times exceeding 4 sec (e.g., curve for VP 2750 in Fig. 5). In view of the good results from the northern recording, the low-quality southern data probably arise from some local effect, such as deep snow or absorptive sediment. Brocher *et al.* (1991) came to a similar conclusion, namely that an inverse relationship exists between the thickness of Cenozoic rocks and the amplitude of seismic signals.

The poor seismic reflection image obtained south of the Denali fault means that neither the deep crustal structure of terranes south of this fault nor the configuration of the Denali and Hines Creek faults are evident in seismic reflection data. No fault-plane reflections reveal the location of either fault, and the appearance of reflections across these faults' surface traces does not change systematically to indicate any major break in the crust.

Coherent seismic reflections begin abruptly at about VP 2400, where the Denali seismic reflection line begins to diverge from the Hines Creek fault (Fig. 4; Plate 1, top). We identify three main reflection bands, labeled A, B, and C (Fig. 6; Plate 1, top). The prominent reflection band A dips north from below the surface trace of the Hines Creek fault, and below VP 3000 this band reaches its greatest travel time of about 3 sec (Fig. 6) and depth of about 7 km (Plate 1, top). Reflection band A and shallower reflections reveal a broad synform with an axis below VP 2950. This axis lies about 5 km south of the axis of an outcropping, east–west syncline that deforms lower Tertiary sedimentary rocks and the compositional layering of metamorphic rocks in the southern YTT (axes shown in Fig. 4). The close spatial association of the two axes suggests that the early Tertiary or younger folding evident in surface rocks also dates the synformal folding of rocks that cause reflection band A.

North of VP 3000, linear reflections begin at the bottom of reflection band A, splay upward to the south, and terminate at a shallower reflection (Fig. 7). These reflections suggest thrust faults confined within an upper-crustal shear zone. This inferred shear zone is folded by the synform described in the preceding paragraph. Other evidence for thrust faulting within rocks that cause reflection band A includes the linear reflections that diverge to the south from the bottom of this reflection band (Fig. 8).

Below VP 2800 an asymmetric antiform is evident below reflection band A, between about 2 and 4 sec (Fig. 6). The south limb of the antiform is the steeper, and this limb ends downward and southward against reflection band B. Projected upward and southward to the surface, the axis of this antiform coincides in location with the axis of the antiform that follows the north side of the Denali fault (axis shown in Figs. 1 and 4). The coincidence of surface and subsurface axes suggests that the subsurface antiform developed during the Cretaceous retrograde metamorphism that produced the surface feature.

Reflections from within the subsurface antiform include strong events that were clearly evident on records examined in the field, before any data processing was performed. We call these events collectively the Denali bright spot. The strongest reflections occur below VP 2750 at about 3 sec (Fig. 8). The migrated image shows that the bright spot is nearly flat. The trace-amplitude plot (VP 2750 in Fig. 5) shows the high strength of the bright-spot reflection relative to other reflections and to ambient noise levels (gray-shaded curve for VP 2200).

Reflection band B begins at about 3.2 sec (Fig. 6) or 10 km (Plate 1, top) below VP 2400. Locally this band dips as steeply as 25° north, and the dip decreases progressively northward. At about 10 km depth, band B includes strong events having four or five reflection peaks, but north of VP 3000 this band widens and its amplitude decreases as it flattens progressively into the middle crust, within the depth range of 17 to 20 km (Plate 1, top).

Reflection band C diverges to the south from beneath reflection band B (8 sec below VP 2800, Fig. 6; 20 km depth on Plate 1, top). These reflection bands diverge where the reflective crustal section is greatly thickened. Reflection band C extends south to where the signal from deep rocks is lost below VP 2500.

Below reflection band C, numerous subhorizontal and discontinuous seismic events are apparent. However, no convincing reflections from the Moho are evident anywhere along the Denali seismic reflection section.

Magnetotelluric Data

Data Acquisition and Processing. Magnetotelluric (MT) data can be modeled to yield the electrical resistivity of the Earth's crust (Vozoff, 1991), as we show in Figure 9, for data obtained along the geophysical transect. During the summer of 2002, long-period MT data were acquired with the Narod Intelligent Magnetotelluric System (NIMS). Data were acquired for oscillation periods from 3 sec to 5000 sec, yielding a depth of investigation greater than 50 km. Hori-

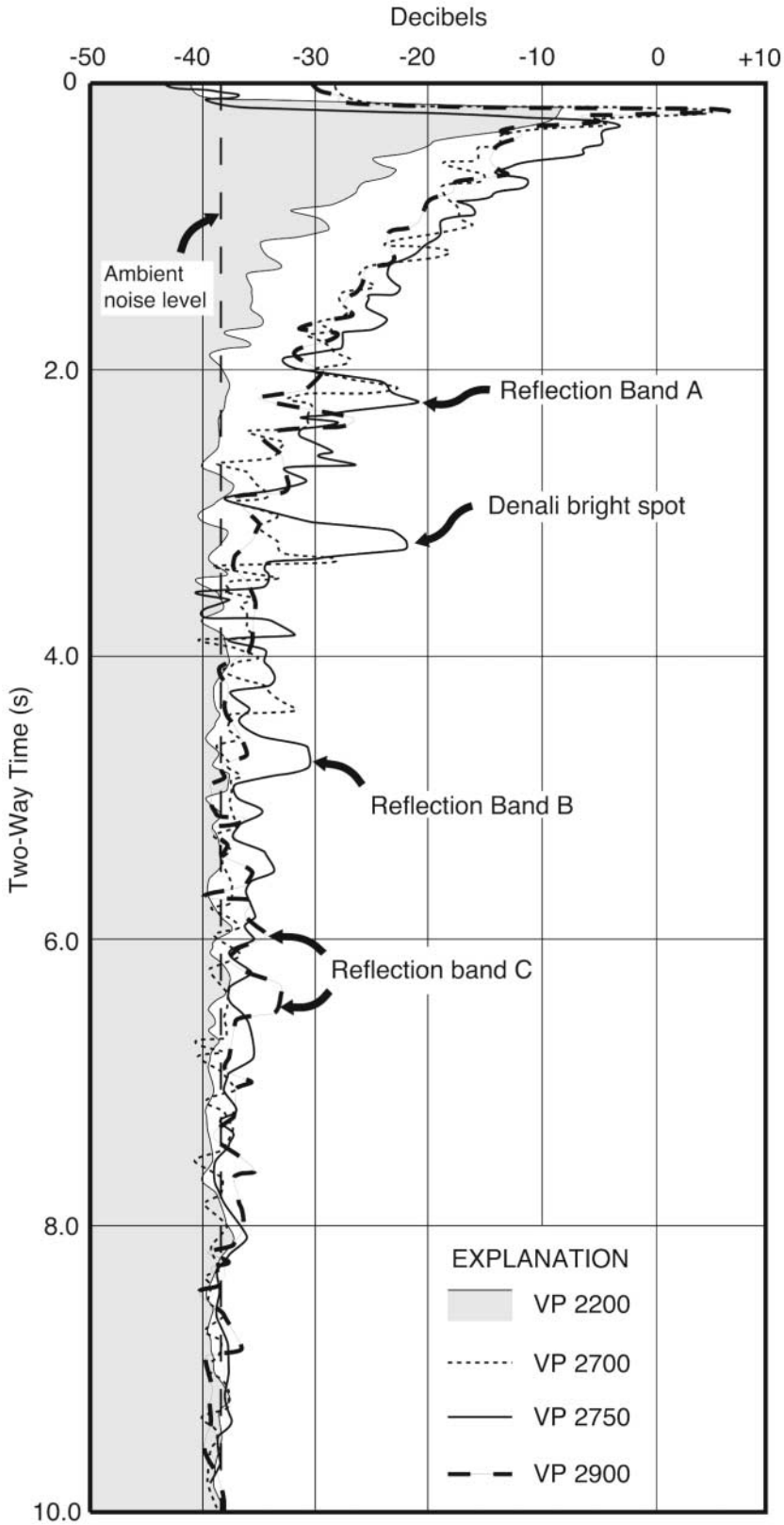

Figure 5. Amplitude variation with travel time for selected seismic traces. Ten traces of stacked seismic data were averaged to calculate each amplitude curve; the amplitudes of stacked data were corrected only for geometric spreading. The curve for VP 2750 shows that the main reflection bands A and B and the Denali bright spot stand out as clear amplitude anomalies.

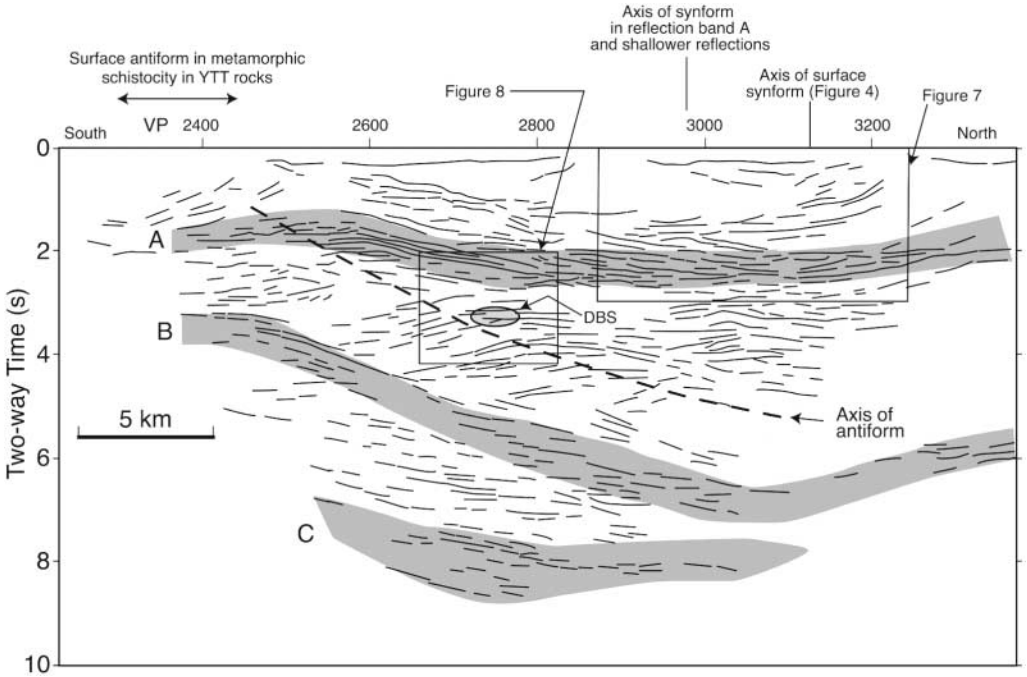

Figure 6. Line drawing of migrated data (versus travel time) showing the three main reflection bands and the axis of the subsurface antiform that projects upward to the south to correlate in location with the axis of an antiform that developed during the Cretaceous.

zontal electric-field data were acquired with electrodes in a cross configuration, and three components of the magnetic field were collected with ring-core sensors in the center of the electrode array. Regional impedance strike is important to modeling MT data, and we assumed a strike value of 115°, but as discussed in the Appendix, the complex geology makes determining this strike problematic.

MT stations were located along the Richardson Highway, across the Denali fault (Fig. 1). Owing to instrument malfunctions, data from only six of eight deployed MT stations were available for interpretation. MT data were processed by using the robust method of Egbert (1997). The processed data, parameterized as apparent resistivity and phase as a function of frequency for each station location, were plotted as pseudosections to show the fit between observed and calculated values (Fig. 10).

MT data for this study are 2D because they were collected along the highway, and especially in the case of 2D data, mode determination is important to MT modeling and interpretation. The transverse magnetic mode (TM) is defined by the electric field being perpendicular and the magnetic field being parallel to strike. The transverse electrical mode (TE) is defined by the electric field being parallel and the magnetic field being perpendicular to strike. Two-dimensional modeling is more robust when the TM mode is used (Wannamaker *et al.*, 1984). For data presented here, the geology is complex, and the MT line is oblique to the regional geologic strike, so rotation of the impedance matrix, discussed more fully in the Appendix, is a reasonable step in data processing and mode identification.

The temporal and spatial sampling of the MT survey described here is suitable to determine deep, large-scale crustal structure, not to characterize the Denali fault in detail. To resolve impedance values within the upper 3–5 km of the Earth's surface, a high-frequency survey would be necessary, so in models shown here, shallow impedance values are shown in muted colors. The sensitivity of MT data to an assumed resistivity model of the crust can be tested by using a suite of inverse models and by means of trial-and-error forward modeling. Both approaches were undertaken for this study, and the details are presented in the Appendix.

The preferred model we use for geologic interpretation (Fig. 9 and Plate 1, bottom) was calculated using the 2D conjugate-gradient inverse algorithm of Rodi and Mackie (2001) from data rotated to principle axes such that the *xy* mode was the TM mode. The model had 88 horizontal and 69 vertical modes. The main departures between observed and calculated values occur for the model parts that represent the Wrangellia terrane and the Denali fault zone.

Results of MT Modeling. The preferred MT model (Fig. 9) reveals four main-rock bodies (R1 through R4). South of the Denali fault, body R1 includes high-resistivity ($>1000\,\Omega\cdot$m) rocks. The north boundary of this body dips about 60° south, and the body extends downward to depths as great as 25 km.

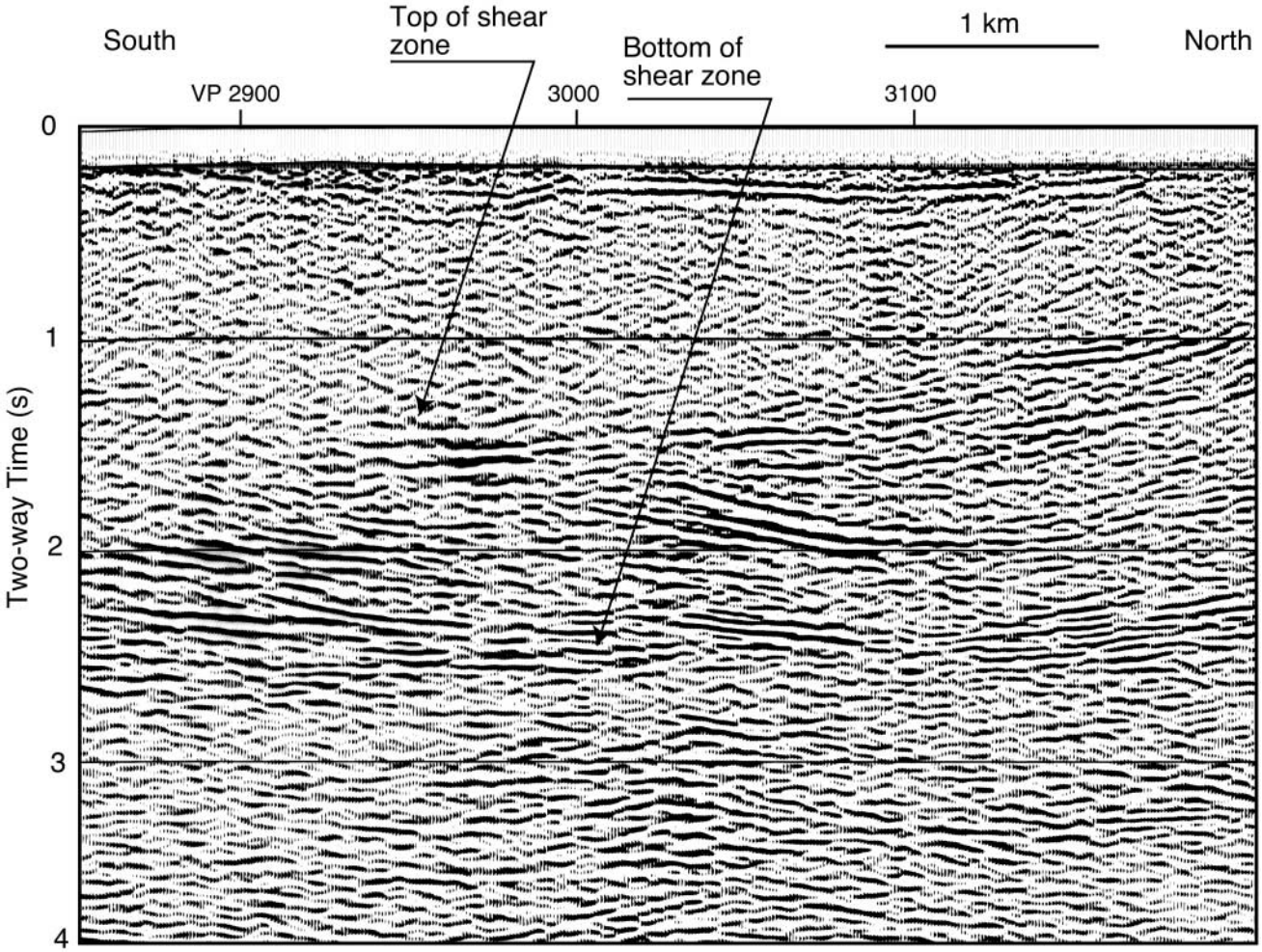

Figure 7. Detail of the migrated Denali seismic section showing the part of reflection band A that outlines the axis of the syncline in early Tertiary sedimentary rocks and in the schistocity of the underlying crystalline rocks of the YTT. The migrated stack (versus travel time) shows reflection band A where this band reveals a duplex structure. Seismic reflections splay upward from the base of this band and terminate at their upper ends at another reflection.

The high-resistivity values that characterize R1 are consistent with unweathered igneous or metamorphic rock like those exposed in the Talkeetna Mountains, east of the Richardson Highway (Glen *et al.*, 2002). Igneous rocks of the Wrangellia terrane are exposed where body R1 is close to the surface.

Body R2 is characterized by low resistivities (about 10 Ω·m) and underlies the Denali and Hines Creek faults. This body is nearly vertical, widens with increasing depth, and appears to extend downward to great depth. Body R3 is moderately resistive (about 300 Ω·m) and extends downward through much of the middle and lower crust. Rocks at the surface above body R3 are YTT metamorphic rocks. Resistivity body R4 (<30 Ω·m) dips north from near the surface into the middle crust. Metamorphic rocks of the YTT crop out where body R4 is shallow.

Previous interpretations of MT data collected along five transects near and across the Alaska Range (Stanley, 1986, 1989; Stanley *et al.*, 1990) indicate a different distribution of rock resistivities from what we show here. In these early studies, a near-surface rock layer north of the Denali fault was found to vary in thickness from 4 to 7 km and to be characterized by a wide range of resistivity values (170–9900 Ω·m) that was identified as the amphibolite-facies schist of the YTT. The prominent feature in the earlier MT models is a thick (20 km), very low resistivity (1–3 Ω·m) rock body that comprises much of the middle and lower crust north of the Denali fault. The most likely source of the low-resistivity body was inferred to be carbon-rich Jurassic and Cretaceous flysch like that making up the Kahiltna terrane.

One difference between the earlier impedance model (Stanley, 1986, 1989; Stanley *et al.*, 1990) and the one presented here (Fig. 9) is that the temporal recording range used to obtain the earlier data was about an order of magnitude

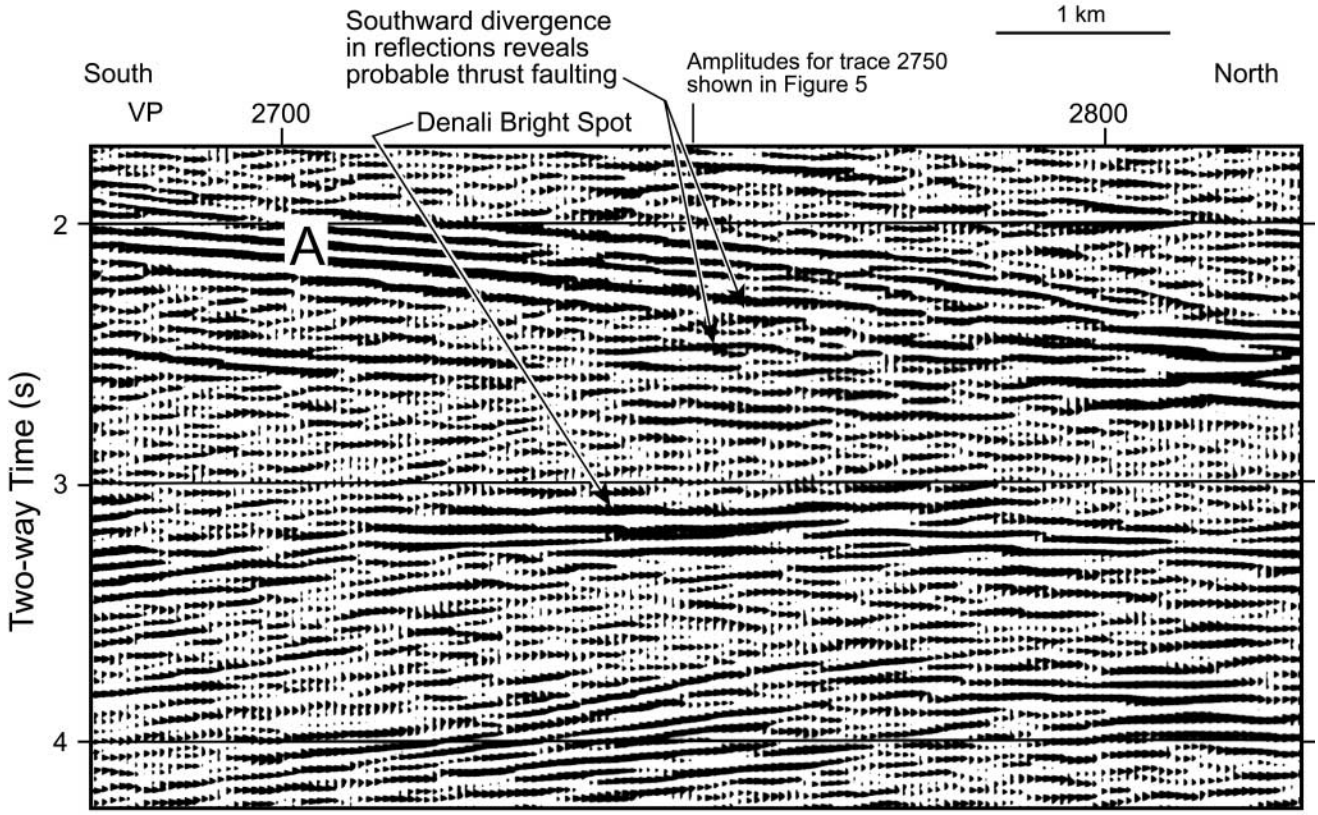

Figure 8. Migrated section showing the horizontal events that make up the Denali bright spot. Reflections that make up reflection band A diverge upward to the south and appear to outline thrust faults.

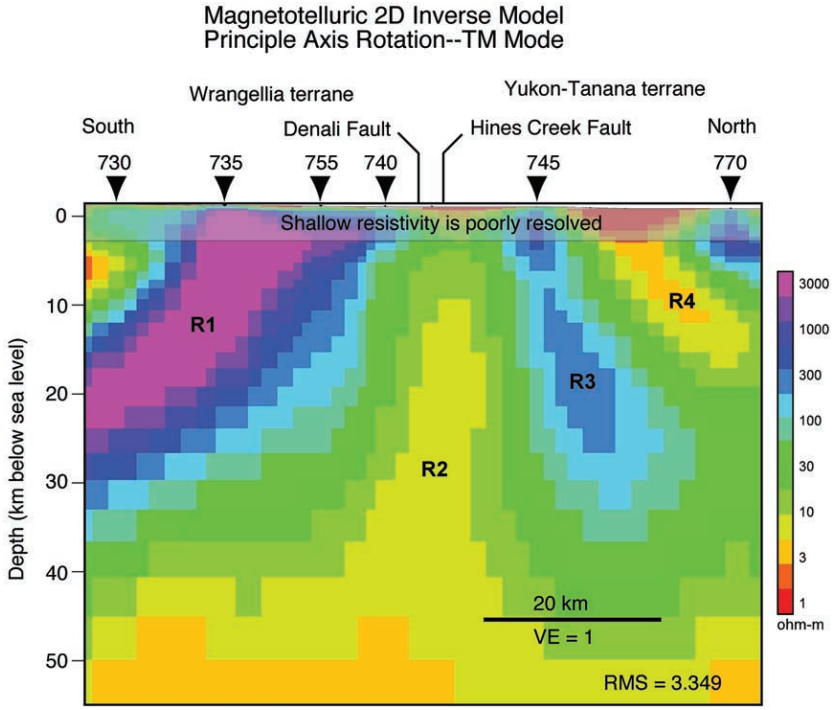

Figure 9. The preferred 2D inverse MT model using the conjugate gradient method for the TM mode from the principle axis rotation.

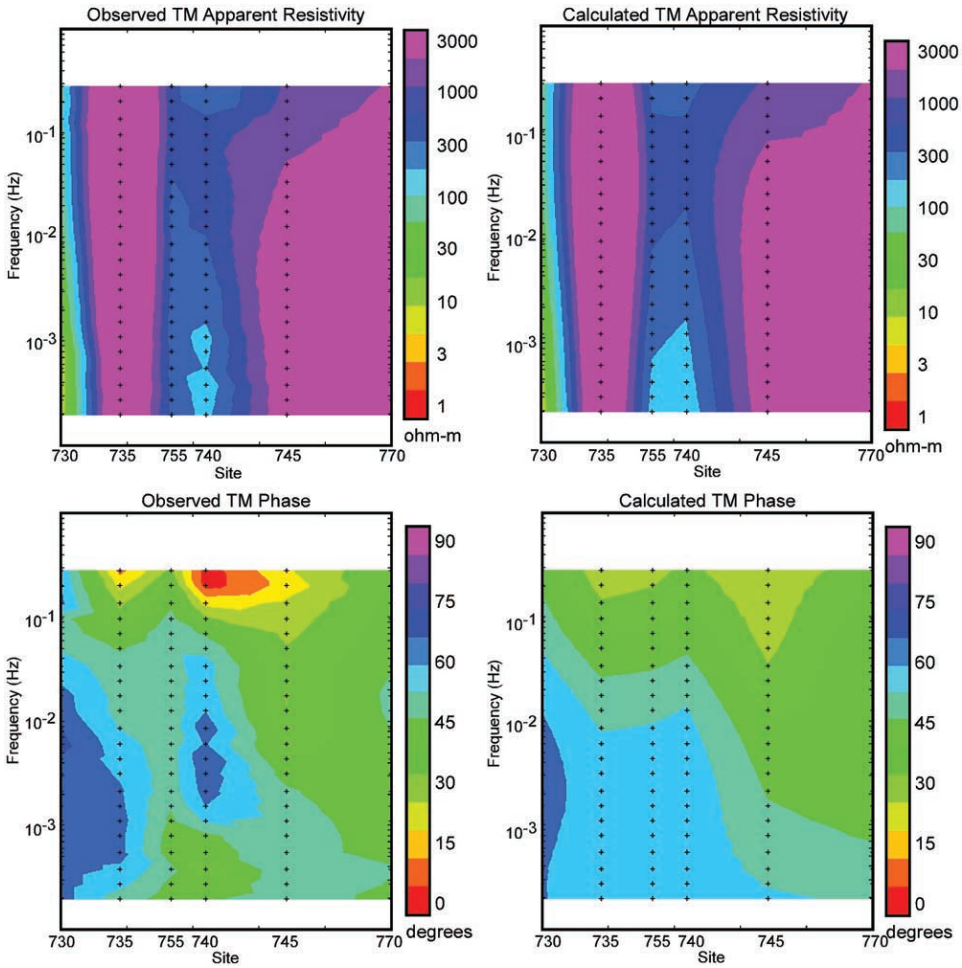

Figure 10. The observed (left) and calculated (right) apparent resistivity (top) and phase (bottom) of the 2D model of Figure 9 presented in pseudosection format to illustrate how observed and calculated values compare.

higher than that used for data shown here. Hence, earlier data focused on the shallow crust. Furthermore, the earlier 2D model was constructed through forward modeling, with a series of 1D models stitched together. Data interpreted with 1D models can be severely distorted by multidimensional effects.

Gravity and Magnetic Data

Data Collection and Processing. Aeromagnetic data were collected during two surveys, one of which covers the entire region represented by Figure 11. During this survey, data were collected 303 m above the ground, with lines oriented north–south and spaced 1.6 km apart (Saltus and Simmons, 1997; survey AK08). The second aeromagnetic survey provided high-resolution data collected 0.06 km above the ground, with lines oriented N30°E and N20°W and spaced 0.2 km and 0.4 km apart (Burns, 2003). The second aeromagnetic survey covers the southern half of the area represented by Figure 11. Gravity data (Morin and Glen, 2002, 2003) were reduced to isostatic-anomaly values, using standard gravity reduction methods (Dobrin and Savit, 1988; Blakely, 1995).

Most of the isolated magnetic peaks south of the Denali fault are caused by the Nikolai greenstone and associated intrusive rocks. These peaks outline Triassic mafic and ultramafic rocks, like the Fish Lake and Tangle Lakes ultramafic complexes (bodies A, H, and I on Fig. 11) and the Rainey and Canwell ultramafic complexes (bodies J and A, respectively, on Fig. 11). These magnetic bodies are likely to be fault bounded, but poor rock exposures in this area limit our ability to specify structural relationships.

The Denali fault is evident in both gravity and magnetic data because the fault is associated with regional gradients that decrease to the north across the fault and distinguish the Wrangellia and Yukon-Tanana terranes (Fig. 11). These gradients amount to 15 mGal and 300 nT over a distance of about 10 km. Across the fault, gravity and magnetic anomalies decrease from high and irregular, on the south, to low and smooth, on the north.

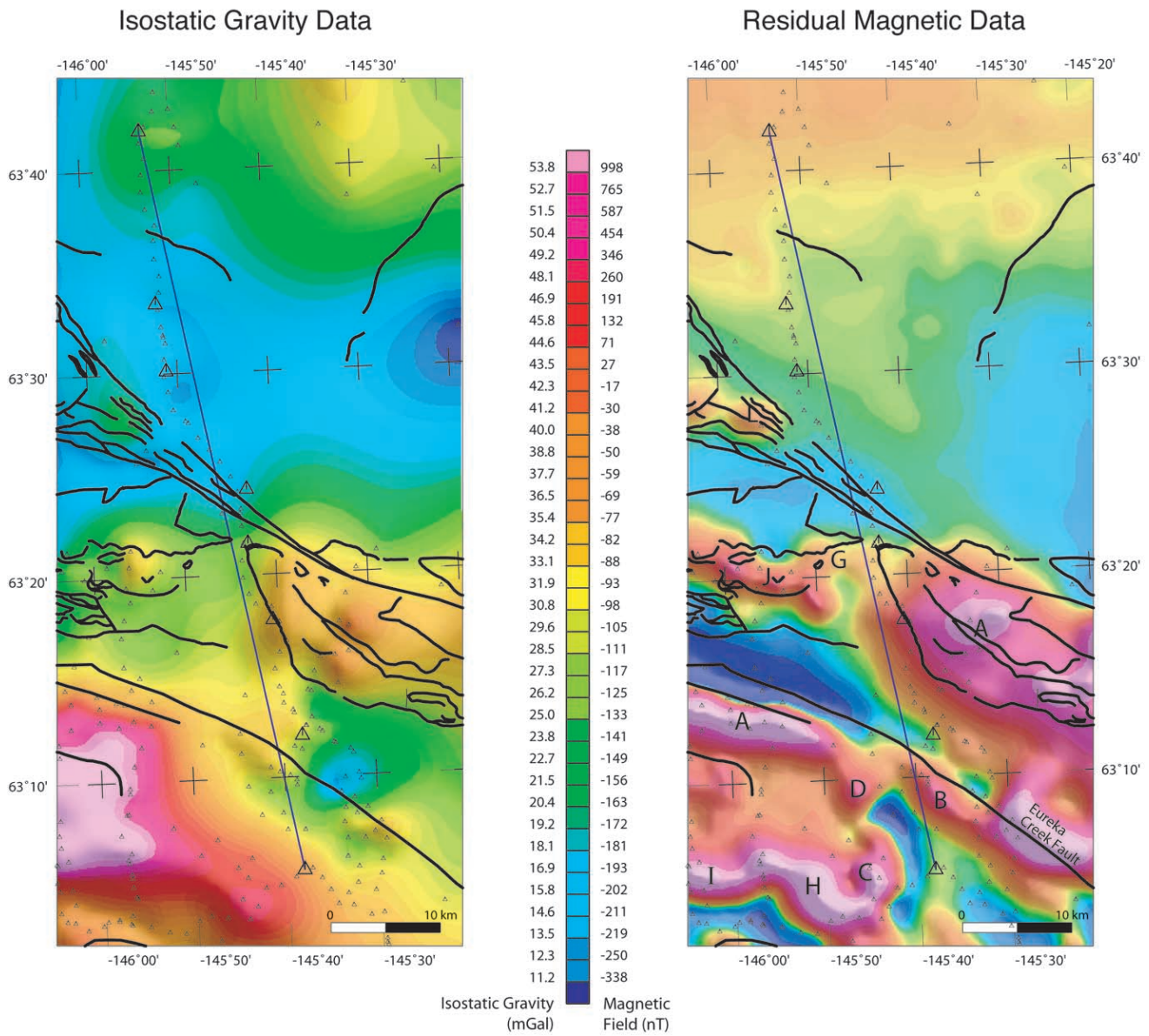

Figure 11. Isostatic gravity (left) and residual magnetic field (right) maps of the study area. Small triangles represent gravity stations and large triangles show MT stations. The blue line shows the potential field profile corresponding to the model shown in Figure 12. Letters refer to features discussed in the text.

Potential Field Modeling. The model profile (Fig. 11) was chosen to parallel as closely as possible the seismic reflection and the MT station lines, and to include the maximum number of gravity stations, which were largely concentrated along the Richardson Highway. The potential field model (Fig. 12) was constructed using a commercially available, 2D forward-modeling system (GMSYS) that allows for source bodies that are not orthogonal to the direction of the model. In the model, source bodies consisted of horizontal tabular prisms aligned with their axes parallel to the regional geologic strike. Each prism has its own strike extent, and prisms were positioned asymmetrically with respect to the profile, when necessary.

We used rock-property data from this and surrounding regions (Campbell and Nokleberg, 1997; Sanger and Glen, 2003) to define the properties of the major rock units that cross or lie near the model profile. Source bodies for magnetic anomalies were assumed to have only induced magnetization; however, magnetic remanence may contribute significantly to the observed magnetic anomalies, in particular, in the mafic and ultramafic rocks associated with the Nikolai Greenstone.

Probably the greatest sources for error in the potential-field models are the discontinuous rock bodies south of the Denali fault and the acute angle between the model's northwest direction and the west-northwest strike of major faults

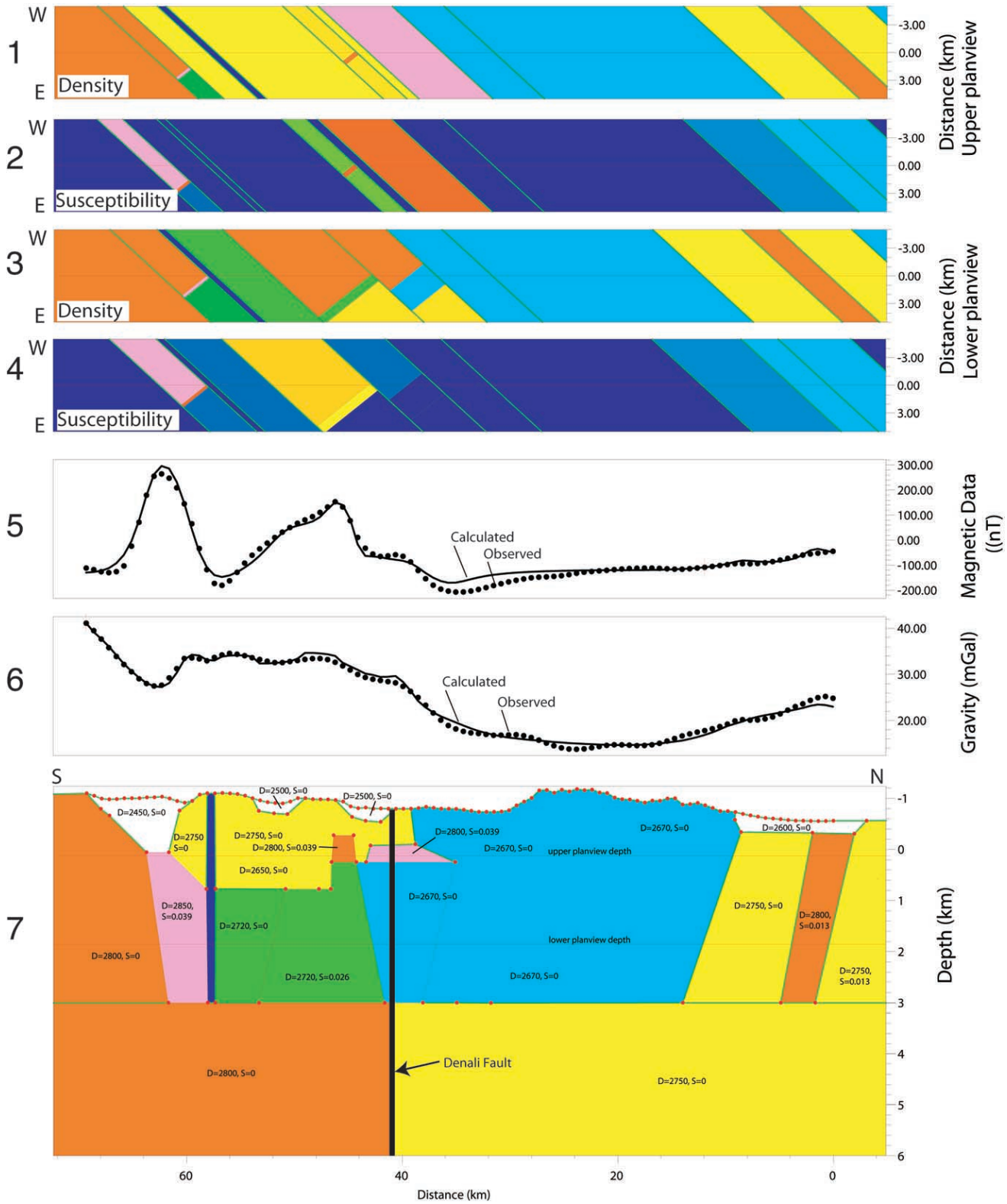

Figure 12. Forward potential-field model corresponding to the line of profile shown in Figure 11. Upper two panels show plan views of the model at an elevation ~130 m below sea level (the first panel is colored by density and the second panel by susceptibility). Third and fourth panels show plan views of the model at an elevation ~1900 m below sea level (the third panel is colored by density and the fourth panel by susceptibility). The slant of model bodies reflects the southeast strike of units. Fifth and sixth panels give observed (filled circles) and model (solid line) anomalies for magnetic and gravity fields, respectively. The seventh panel shows a cross section of the model. Note that some of the bodies shown on the cross section do not actually cross the profile; their positions relative to the profile are depicted in the upper four panels. Numbers associated with the model bodies (bottom panel) give the model density (kg/m^3) and magnetic susceptibility (SI).

and rock units. In particular, the high magnetic and gravity peaks measured over the Wrangellia terrane cause much uncertainty in data interpretation because they have out-of-plane sources. In constructing the model, the crust between 3 and 10 km was defined by two regional blocks to distinguish the relatively dense Wrangellia terrane from the less dense YTT. These regional bodies meet along a vertical boundary that emerges at the surface along the trace of the Denali fault. Shallow crustal bodies were modeled assuming their bottoms lay at a depth of 3 km.

For our purposes, anomalies produced by the shallow rock bodies south of the Denali fault are noise that prevents us from examining the deep crust. The goals of our potential-field modeling were, first, to determine whether bodies in the shallow crust could account for the complex gravity and magnetic fields measured over the Wrangellia terrane, and second, to extract what information we could about deeper crustal levels and especially about the deep configuration of the Denali fault. Despite the modeling uncertainties, we propose that the majority of the strong magnetic anomalies are accounted for by shallow (<3 km) sources. In addition, the Denali fault appears to dip steeply down to a depth of about 10 km.

Integration of Geophysical Data Sets

The main correlations from an integrated interpretation of geologic and geophysical data are:

1. Gravity and magnetic data can be modeled to indicate that the Denali fault dips steeply to depths of about 10 km. In addition, MT data show the vertical, low-resistivity body R2 below this fault's surface trace. These findings suggest the Denali fault dips steeply to vertically below the geophysical transect. Although by themselves these findings are ambiguous, they agree with the results of modeling of InSAR data from an area 100 km west of the geophysical transect. This modeling reveals a steeply dipping (81°) fault. Furthermore, modeling of GPS data proceeded on the basis of a vertical fault because teleseismic waveform data indicate a steeply dipping (86°) fault.
2. Seismicity and strong seismic reflectivity do not correlate in location (Plate 1, bottom). Hypocenters tend to fall closely along the Denali fault, and only scattered hypocenters north of this fault occur along the strong seismic reflectors that are shallower than the 10 km seismicity cutoff. Furthermore, north of the fault seismic reflections mainly dip north, whereas alignments in aftershock hypocenters dip south toward the fault (Fig. 3). These relationships mean that reflective features above the 10 km have been essentially aseismic since 1975.
3. Igneous rocks of the Wrangellia terrane are nonreflective, have high electrical resistivities (body R1), and cause high-amplitude and variable, gravity, and magnetic anomalies. The north boundary of resistivity body R1 dips steeply (60°) south and may delimit the Wrangellia terrane on the north.
4. The surface trace of the Denali fault nearly bisects low-resistivity body R2. The lowest-resistivity part of this body occurs deeper than about 10 km, which is below the regional maximum aftershock depth of 10 km. Rocks forming body R2 are poorly reflective, and gravity and magnetic anomalies decrease smoothly northward across this body.
5. MT and seismic reflection data show that the north and upper boundary of moderately resistive body R3 coincides with reflection band B (Plate 1, bottom). Rocks at the surface above resistivity body R3 are strongly metamorphosed sedimentary and volcanic units of the YTT. Body R3 is not associated with gravity or magnetic anomalies; even so, rocks in this body differ in physical properties from their encasing rocks, as indicated by the contrast in electrical resistivity and the reflection from along the body's top.
6. The strong reflections we call the Denali bright spot come from rocks within the resistivity gradient between bodies R3 (moderate resistivity) and R4 (low resistivity). The subhorizontal reflection band A stems from rocks within low-resistivity body R4. Hence, except for reflection band B, which lies along the top of body R3, the reflection bands are not closely tied to the resistivity distribution.
7. The axis of the antiform in retrograde metamorphic YTT rocks (axis shown in Fig. 1 and 4) crosses the geophysical transect near VP 2400 (Plate 1). This axis coincides in location with where the subsurface antiform between reflection bands A and B projects to the surface. Both the surface antiform and the upper part of the arched reflection bands fall within resistivity body R3 where this body extends to shallow depth.
8. The surface syncline in early Tertiary rocks (VP 3150 on Fig. 4) correlates in location with a synform at depth that deformed reflection band A.

Discussion

Causes for Variation in Crustal Resistivity

Jones (1989) advocated joint interpretation of seismic reflection and MT data and indicated that low-resistivity rocks that are acoustically transparent are challenging to interpret. Low-resistivity body R2 falls within this category. This body is intriguing not only because of its low resistivity but also for its location beneath the surface trace of the Denali fault. The source of low-resistivity values for body R2 is difficult to constrain because possible sources include metallic sulfides, partial melt, carbon films, and aqueous fluids. Sulfide mineralization is locally present in the study area (Carlson and Hulbert, 2002), but a rock mass the size of body R2 would require prodigious amounts of sulfides for such minerals to be the sole cause of the low resistivity. Partial

melt is also an unlikely cause for the low resistivity because Quaternary volcanism is unknown in the study area.

Carbon films in low-grade metamorphic rocks can cause low electrical resistivities (Wannamaker, 1986; Wannamaker *et al.*, 2002). At low metamorphic grades, carbon particles in these rocks can be smeared into films that are electrically conductive. Below the Alaska Range, carbon-rich rocks, like the Upper Jurassic and Lower Cretaceous flysch within the Kahiltna and related terranes, could have been buried during mountain building (Stanley, 1989; Stanley *et al.*, 1990). Although intense heating and deformation can destroy carbon films, high-grade metamorphic rocks in the YTT do contain such films (Mathez *et al.*, 1995).

Aqueous fluids can also produce low electrical resistivities, and the Denali bright spot might be evidence for aqueous fluids in the middle crust. Hyndman and Shearer (1989) and Pratt *et al.* (1991) indicate that midcrustal bright spots in seismic reflection data can be caused by magma, acoustic tuning in rock layers, and fluids. The Denali bright spot is flat and discordant to the antiform outlined by other nearby reflections. This discordance indicates that fluids cause the bright spot because the other likely cause, acoustic tuning in rock layering, would most likely produce reflections that are concordant with the antiform.

Geologic Structure Inferred from MT Data

The MT signatures of other strike-slip faults show vertical, low-resistivity bodies below the faults. The Denali fault may be analogous tectonically to the Altyn Tagh fault of Tibet, because both faults are thought to facilitate the tectonic escape of large crustal blocks (Eberhart-Phillips *et al.*, 2003). An MT survey over the Altyn Tagh fault revealed a rock mass with resistivities as low as 10 $\Omega\cdot$m that locally reaches the surface but mainly extends vertically downward from about 4 km to the maximum modeled depth of 8 km (Bedrosian *et al.*, 2001). The preferred interpretation is that the low-resistivity body indicates carbon-rich marine sedimentary rocks. MT surveys across the Southern Alps of New Zealand (Wannamaker *et al.*, 2002), over strike-slip faults in the Basin and Range province of eastern California (Park and Wernicke, 2003), and across the San Andreas fault in California (Unsworth *et al.*, 1997, 1999, 2000; Bedrosian *et al.*, 2002) associate these faults with vertical zones having low resistivity and considerable (>5 km) depth extent.

Thus, our findings about body R2 near the Denali fault conform with general findings about other strike-slip faults. Hence, we propose that this body indicates the subsurface location of the Denali fault. Although some studies indicate that carbon films are responsible for the low resistivities of the vertical bodies (e.g., Bedrosian *et al.*, 2002), most studies highlight the role of fluids.

A Structural Model of the Aftershock Zone of the Denali Fault Earthquake

We propose a crustal-structure model of the Alaska Range orogen by assuming a two-phase geologic history that is simplified from discussion in Nokleberg *et al.* (1994) and Ridgway *et al.* (2002). The first phase occurred during the Late Cretaceous and Early Cenozoic, when an oblique-convergent plate boundary lay near what would later become the strike-slip Denali fault. The second phase involved Cenozoic strike-slip offset along this fault.

In our interpretation, during the first (Late Cretaceous and Early Cenozoic) phase, reflection band B formed within the upper plate of the oblique-convergent plate boundary as Wrangellia and other terranes collided with Alaska. The age of the reflective features is inferred, as described previously, from correlating the surface antiform that developed during Late Cretaceous (~105 Ma) retrograde metamorphism with the subsurface antiform evident in seismic reflection data.

The sigmoid shape of reflection band B and the divergence between reflection bands B and C (Fig. 6; Plate 1, top) suggest that they form a crustal-scale duplex structure (Iverson and Smithson, 1983a,b; Smithson *et al.*, 1986; Le Gall, 1990) that soles out northward into the middle crust at about 20 km depth (Fig. 13). Reflection bands B and C partly outline resistivity body R3, and because this body underlies the surface antiform in YTT rocks, we propose that this body's emplacement caused the antiform to develop. If so, then body R3 and its associated reflections reveal structures that are about 105 Ma old, the time of retrograde metamorphism of antiformal surface rocks.

The lithologies that make up this proposed duplex structure are unknown. However, body R3, which makes up most of this structure (Fig. 13), does not include a flap of lower-crustal or upper-mantle material incorporated into the Alaska Range orogen because both gravity and magnetic values are low and smooth over this body (Fig. 13; Plate 1, bottom).

Rocks that cause reflection band B are an important element in the crustal structure of the Alaska Range; these reflective rocks thicken downward and flatten northward within the depth range of 17 to 20 km (Plate 1, top; Fig. 13). This shape probably reveals the ramp of a crustal-scale shear zone, as has been suggested for hinterland-dipping reflections from other compressional orogens (Ando *et al.*, 1984; Allmendinger *et al.*, 1987; Eisbacher *et al.*, 1989; Gray *et al.*, 1991; Cook and Varsek, 1994; Beaumont and Quinlan, 1994). This reflection band thickens with increasing depth, a common attribute of crustal-scale faults (Sibson, 1982; Smithson *et al.*, 1986).

Given the high metamorphic grade of surface rocks, the reflection bands most likely reveal ductile shear zones, perhaps ones that developed according to kinematic models of oblique-convergent margins (e.g., Fitch, 1972; Beck, 1983; Chemenda *et al.*, 2000). Parts of these ductile zones, however, are now within the brittle deformation regime, which extends downward to about 10 km, the maximum depth of aftershocks along the Denali fault (Ratchkovski *et al.*, 2003). In particular, all of reflection band A and the upper part of band B are shallower than this depth.

In our model for the development of the Denali fault, the later phase of deformation along this fault occurred dur-

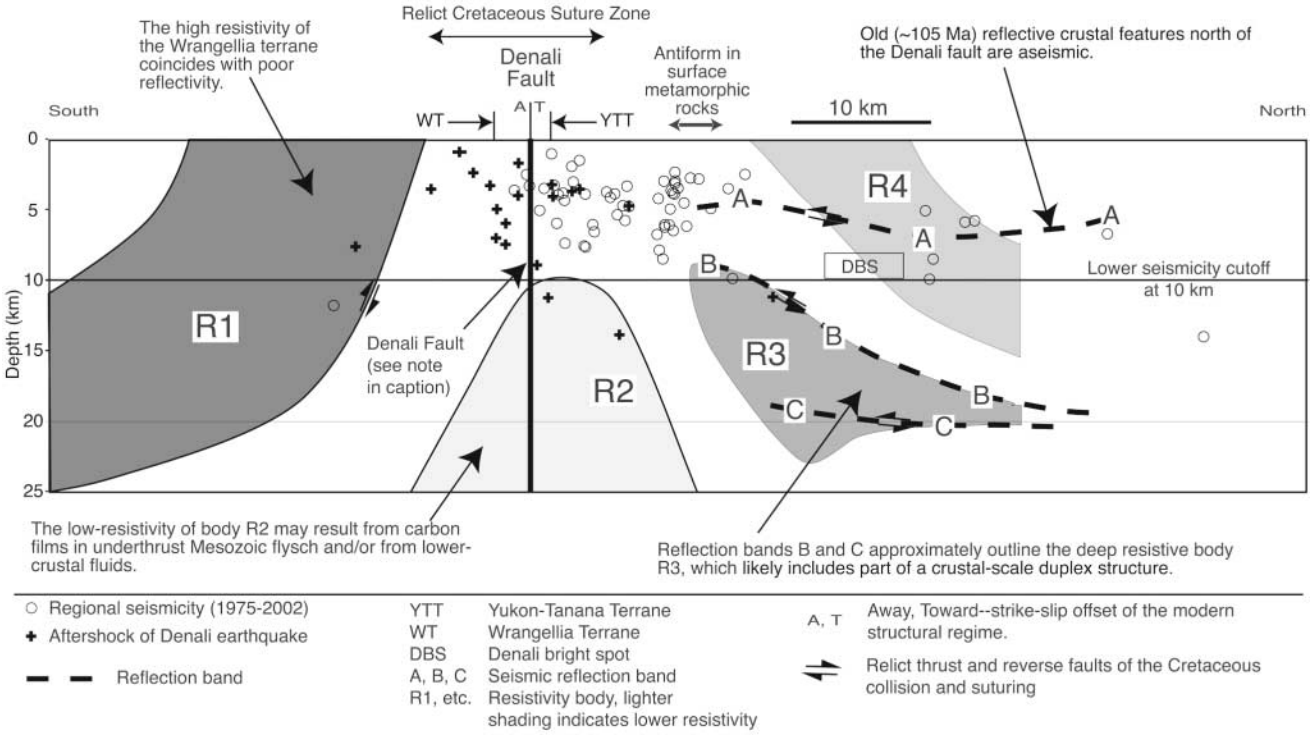

Figure 13. Structural model of the Alaska Range orogen and aftershock zone of the Denali fault earthquake. Opposed thrusting developed during late Cretaceous terrane collision, involving Wrangellia and an oblique-convergent margin along what was then the south and west margin of Alaska. Structures revealed by seismic reflection data are mostly aseismic, but the lower cutoff for seismicity is at the shallow depth of only 10 km, so some of these features could support ductile strain. Low-resistivity rocks in body R2 underlie the surface trace of the Denali fault and may indicate this fault's position in the deep subsurface. The cause for the low resistivity is unknown but likely results from carbon films or fluids.

ing the Early Cenozoic. At this time, structures developed during the first phase of deformation were overprinted as the present strike-slip Denali fault began to form in response to a change in North Pacific plate motions (Nokleberg *et al.*, 1994; Ridgway *et al.*, 2002). Seismic reflection data provide no evidence for this overprinting. This accords with common findings about strike-slip faults, especially ones in crystalline terranes, which usually produce only muted, indirect responses in seismic reflection data, involving zones of poor reflection quality that are 5–20 km wide (Lemiszki and Brown, 1988). In the Alaska Range, other faults evident in outcrops north and south of the Denali fault, and especially west of the geophysical transect, were active during the Cenozoic and are believed to form a positive flower structure (as defined in Harding, 1985) that records Cenozoic transpression across the Denali fault (Nokleberg *et al.*, 1985, 1989).

In an alternative structural model, the Denali fault does not dip steeply but instead is low angle and merges downward and northward with the shear zone that causes reflection band B. The fault then would flatten at 20 km depth, into what are probably ductile rocks. One problem with correlating the fault with the reflection band is that part of the band extends above the 10 km seismicity cutoff, and this part is close to the Denali fault's surface trace. If the correlation were correct, this part of the band should have been seismically active. For the same reason, the Denali fault cannot merge with reflection band A because rocks that cause this band remain above the lower seismicity cutoff. The discordance in dip between hypocenter alignments and seismic reflections also makes this alternative structural model unlikely.

South of the Denali fault, the shallow part of resistivity body R1 correlates in location with volcanic and plutonic rocks of the Wrangellia terrane. Although modeling of complicated gravity and magnetic anomalies measured south of the Denali fault (Fig. 12) does not reveal features that penetrate deeply into the crust, modeling of MT data indicates that the north boundary of body R1 dips steeply south and extends to depths near 20 km. We interpret this boundary as a thrust fault that formed when the Wrangellia terrane collided with Alaska.

In our preferred crustal structure model for the aftershock zone, the strike-slip Denali fault dips steeply to vertically and extends to depths of about 30 km (Fig. 13). This fault is sandwiched within an old suture zone, where struc-

tural remnants of opposed late Cretaceous and early Cenozoic thrusting penetrate deeply (20 km) into the crust. Judging from the sparse hypocenters that occurred shallower than the 10-km seismicity cutoff and more than 10 km perpendicularly away from the Denali fault (Plate 1, bottom), we propose that the highly reflective crustal features north of this fault are relict and are not involved in modern seismicity. Similarly, the absence of seismicity along the north boundary of body R1 shallower than 10 km indicates that it, too, is relict.

Relating Earthquakes to Crustal Structure

We compare the preferred structure model (Fig. 13) with sections showing aftershock hypocenters (Fig. 2) to derive a possible configuration of seismogenic structures along the Denali fault (Fig. 14). Locally, aftershock hypocenters are aligned and dip toward the surface trace of the Denali fault. The hypocenter alignments are interpreted to fall along oblique-slip faults similar to the Hines Creek fault. The distribution of aftershock events in map view (Fig. 1) indicates that the oblique-slip faults have limited extent (10–20 km) along strike. Because many faults west of the Richardson Highway converge with the Denali fault, the faults interpreted to make up the flower structure west of this highway are not likely to be continuous with interpreted faults east of the highway.

In many areas, the maximum depth of seismicity lies between 15 km and 20 km, where rock temperature is between 350 and 400°C (e.g., Sibson, 1982; Williams *et al.*,

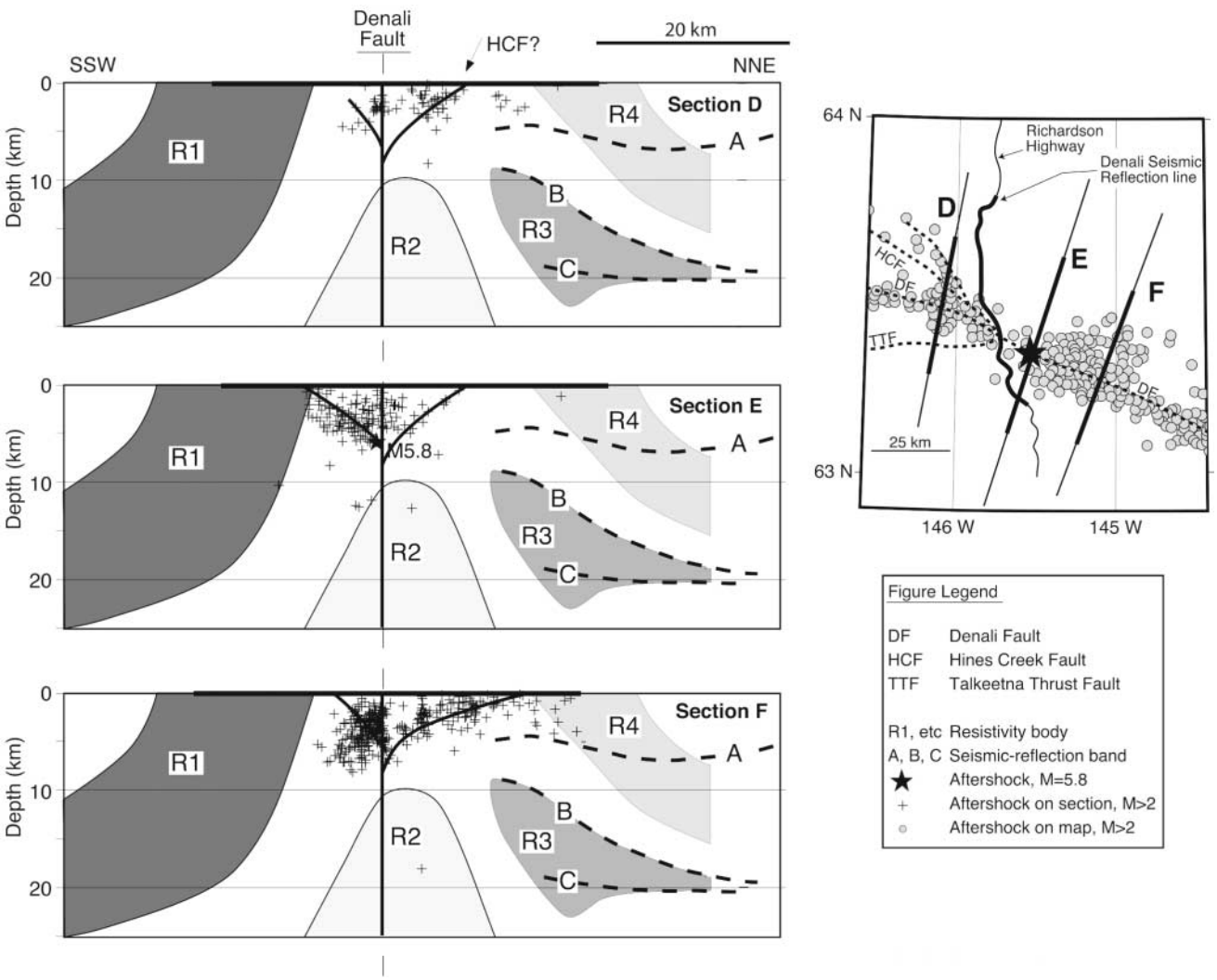

Figure 14. Three hypocenter cross sections (same as in Fig. 3) perpendicular to the Denali fault, showing the highly variable distribution along the Denali fault of aftershock events from the Denali fault earthquake. Also shown are the main features interpreted from geophysical data (Fig. 13). In making this figure, aftershock hypocenters were projected parallel to the Denali fault onto the cross section (Fig. 13) that obliquely crosses the fault (index map). The Denali fault is interpreted to lie within a flower structure as defined by the heavy black lines.

2001; Bonner *et al.*, 2003). Along the Denali fault, a temperature-dependent seismicity cutoff for aftershocks at 10 km depth would indicate a higher-than-normal geothermal gradient. Geothermal data are lacking from the study area. Hot springs are one possible indicator of a high geothermal gradient, and such springs are abundant north of Fairbanks but are uncommon south of this city (Miller, 1994). Even so, one possibility is that shallow seismicity along the Denali fault results from a higher than normal geothermal gradient, and the distribution of earthquakes in depth might not be influenced by the presence of body R2.

Whether body R2 controls the distribution of seismicity along the Denali fault depends on the cause for the low electrical resistivity. One possibility is that carbon films in late Mesozoic flysch in the Kahiltna terrane cause the low resistivity. In map view (Fig. 1) these rocks terminate to the northeast against the Denali fault near the intersection of the fault and the geophysical transect. Body R2, then, might represent the subsurface truncation of this flysch basin along the Denali fault. Carbon-rich flysch would seem to have little bearing on the seismicity distribution.

On the other hand, crustal fluids may cause the low resistivity of body R2. In support of this contention, we note that the Denali bright spot occurs in the midcrust north of the Denali fault, and Smithson *et al.* (2000) stress the importance of fluids in producing strong seismic reflectivity. If body R2 does contain fluids, they could have an important influence on the seismicity distribution by weakening the middle and lower crust along the Denali fault, so that tectonic stress is borne by the relatively thin and brittle part of the crust shallower than 10 km. If these fluids were to extend above the 10 km aftershock cutoff, they could reduce rock friction (Byerlee, 1990, 1993) and help localize seismicity.

Conclusion

Low-resistivity body R2 underlies the surface trace of the Denali fault, and similar bodies have been found along other strike-slip faults; we therefore propose that body R2 shows the location of the Denali fault downward through the crust. Gravity and magnetic data can be interpreted to indicate that the Denali fault is vertical to a depth of about 10 km. A vertical fault also conforms with assumptions and findings in the modeling of InSAR and GPS data. We use this body of inference to suggest that the Denali fault dips steeply to vertically down to depths of about 30 km.

Strong reflection bands outline resistivity body R3, which we propose to be part of a crustal scale duplex structure that formed during late Cretaceous terrane collision along the ancestral Denali fault. The late Cretaceous date results from projecting the axis of a subsurface antiform, revealed by seismic reflection data, upward to the surface, where an antiform deforms the schistocity of metamorphic rocks. This coincidence in location of axes suggests that the subsurface antiform developed during the Late Cretaceous (105 m.y.).

In our preferred structural model the present vertical strike-slip Denali fault formed within a late Cretaceous collision and suture zone that involved oppositely directed thrust faults. Given the high metamorphic grade of YTT rocks at the surface, seismically reflective features most likely formed during the collision as ductile shear zones. Few hypocenters occurred along the parts of these reflective features that are shallower than 10 km, the regional lower limit of aftershock seismicity. Given the discordant dips of hypocenter alignments and reflective features, the proposed shear zones most likely are seismically inactive and are relict features of late Cretaceous terrane amalgamation.

The Denali bright spot indicates fluids in the crust, so the low-resistivity of body R2 under the Denali fault may be due to fluids. This could have an important influence on seismicity; deep fluids along the Denali fault could weaken the lower crust and localize seismicity within the upper, relatively thin and brittle part of the crust.

Acknowledgments

We thank Tom Parsons and Victor Labson (both U.S. Geological Survey) for supporting this research. We also thank Stephanie Ross and Victoria Langenheim (USGS) for technical reviews of early versions of this report. Two anonymous reviewers were of great assistance. The Trans-Alaska Crustal Transect (TACT) project, active during the 1980s, provided data, support, and ideas that aided the investigation described in this report. The main TACT participants included Bruce Beaudoin, David Campbell, Nicholas Christensen, Gary Fuis, Victor Labson, Alan Levander, Walter Mooney, Robert Page, George Plafker, and Dal Stanley. The NIMS MT data were acquired by Alisa Green, Colorado School of Mines, and processed by John Booker of the University of Washington.

References

Aleinikoff, J. N. (1984). Age and origin of metaigneous rocks from terranes north and south of the Denali fault, Mt. Hayes quadrangle, east-central Alaska, *Geol. Soc. Am. Abstr. Prog.* **16,** 266.

Aleinikoff, J. N., and W. J. Nokleberg (1985). Age of Devonian igneous-arc terranes in the northern Mount Hayes quadrangle, eastern Alaska Range, *U.S. Geol. Surv. Circular 967*, 44–49.

Aleinikoff, J. N., C. Dusel-Bacon, and H. L. Foster (1986). Geochronology of augen gneiss and related rocks, YTT, east-central Alaska, *Geol. Soc. Am. Bull.* **97,** 626–637.

Allmendinger, R. W., K. D. Nelson, C. J. Potter, M. Barazangi, L. D. Brown, and J. E. Oliver (1987). Deep seismic reflection characteristics of the continental crust, *Geology* **15,** 304–309.

Ando, C. J., B. L. Czuchra, S. L. Klemperer, L. D. Brown, M. J. Cheadle, F. A. Cook, J. E. Oliver, S. Kaufman, T. Walsh, J. B. Thompson, J. B. Lyons, and J. L. Rosenfeld (1984). Crustal profile of mountain belt: COCORP deep seismic reflection profiling in New England Appalachians and implications for architecture of convergent mountain chains, *Am. Assoc. Petrol. Geol. Bull.* **68,** 819–837.

Backus, G. E., and J. F. Gilbert (1967). Numerical application of a formalism for geophysical inverse problems, *Geophys. J. R. Astr. Soc.* **13,** 247–276.

Beaudoin, B., G. S. Fuis, W. D. Mooney, W. J. Nokleberg, and N. I. Christensen (1992). Thin, low-velocity crust beneath the southern YTT, east-central Alaska: results from Trans-Alaska Crustal Transect refraction/wide-angle reflection data, *J. Geophys. Res.* **97,** 1921–1942.

Beaumont, C., and G. Quinlan (1994). A geodynamic framework for in-

terpreting crustal-scale seismic reflectivity patterns in compressional orogens, *Geophys. J. Int.* **116,** 754–783.

Beck, M. E. (1983). On the mechanism of tectonic transport in zones of oblique subduction, *Tectonophysics* **93,** 1–11.

Bedrosian, P. A., M. J. Unsworth, and G. Egbert (2002). Magnetotelluric imaging of the creeping segment of the San Andreas fault near Hollister, *Geophys. Res. Lett.* **29,** 1-1–1-4.

Blakely, R. J. (1995). *Potential Theory in Gravity and Magnetic Applications*, Cambridge U. Press, New York, 441.

Bond, G. C. (1973). A late Paleozoic volcanic arc in the eastern Alaska Range, Alaska, *J. Geol.* **81,** 557–575.

Bond, G. C. (1976). Recognition of a Late Paleozoic marine volcanic arc system in the eastern Alaska Range, in *Recent and Ancient Sedimentary Environments in Alaska*, T. P. Miller (Editor), Alaska Geol. Soc, Anchorage, Alaska, 13.

Bonner, J. L., D. D. Blackwell, and E. T. Herrin (2003). Thermal constraints on earthquake depths in California, *Bull. Seism. Soc. Am.* **93,** 2333–2354.

Brocher, T. M., W. J. Nokleberg, N. I. Christensen, W. J. Lutter, E. L. Geist, and M. A. Fisher (1991). Seismic reflection/refraction mapping of faulting and regional dips in the eastern Alaska Range, *J. Geophys. Res.* **96,** 10,233–10,249.

Brogan, G. E., L. S. Cluff, M. K. Korringa, and D. B. Slemmons (1975). Active faults of Alaska, *Tectonophysics* **29,** 73–85.

Burns, L. E. (2003). Portfolio of aeromagnetic and resistivity maps of the southern Delta River area, east-central Alaska, Alaska Division of Geological and Geophysical Surveys, Geophysical Report 2003-08, 15 pp.

Byerlee, J. (1990). Friction, overpressure and fault normal compression, *Geophys. Res. Lett.* **17,** 2109–2122.

Byerlee, J. (1993). Model for episodic flow of high-pressure water in fault zones before earthquakes, *Geology* **21,** 303–306.

Campbell, D. L., and W. J. Nokleberg (1997). Interpretation of aeromagnetic map and related geophysical data for Mount Hayes 1 degrees × 3 degrees quadrangle, Alaska, *U.S. Geol. Surv. Open-File Rept. 97-0280*, 64 pp., 2 sheets.

Carlson, G. C., and L. Hulbert (2002). Potential for a Noril'sk-type nickel-copper-PGE discovery at Nevada Star's MAN Project, AK (abstract), NW Mining Association 108th Annual Meeting, 16.

Chemenda, A., S. Lallemand, and A. Bokun (2000). Strain partitioning and interplate friction in oblique subduction zones; constraints provided by experimental modeling, *J. Geophys. Res.* **105,** 5567–5581.

Cook, F. A., and J. L. Varsek (1994). Orogen-scale decollements, *Rev. Geophys.* **32,** 37–60.

Csejtey, B. J., D. Cox, R. C. Evarts, G. D. Stricker, and H. L. Foster (1982). The Cenozoic Denali fault system and the Cretaceous accretionary development of southern Alaska, *J. Geophys. Res.* **87,** 3741–3754.

de Groot-Hedlin, C., and S. C. Constable (1990). Occam's inversion to generate smooth, two-dimensional models from magnetotelluric data, *Geophysics* **55,** 1613–1624.

Dobrin, M. B., and C. H. Savit (1988). *Introduction to Geophysical Prospecting*, 4th Ed., McGraw-Hill, New York, 867.

Dreger, D. S., D. Oglesby, R. Harris, N. Ratchkovski, and R. Hansen (2004). Kinematic and dynamic rupture models of the November 3, 2002 M_w 7.9 Denali, Alaska, earthquake, *Geophys. Res. Lett.* doi 10.129/2003GL018333.

Dusel-Bacon, C. (1991). Metamorphic history of Alaska, *U.S. Geol. Surv. Open-File Rept. 91-556*, 48.

Eberhart-Phillips, D., P. J. Haeussler, J. T. Freymueller, A. D. Frankel, C. Rubin, P. Craw, N. A. Ratchkovski, G. Anderson, G. A. Carver, A. J. Crone, T. E. Dawson, H. Fletcher, R. Hansen, E. L. Harp, R. A. Harris, D. P. Hill, S. Hreinsdóttir, R. W. Jibson, L. N. Jones, R. Kayen, D. K. Keefer, C. F. Larsen, S. C. Moran, S. F. Personius, G. Plafker, B. Sherrod, K. Sieh, N. Sitar, and W. Wallace (2003). The 2002 Denali fault earthquake, Alaska: a large magnitude, slip-partitioned event, *Science* **300,** 1113–1118.

Egbert, G. (1997). Robust multiple stations magnetotelluric data processing, *Geophys. J. Int.* **130,** 475–496.

Eisbacher, G. H., E. Lueschen, and F. Wickert (1989). Crustal-scale thrusting and extension in the Hercynian Schwarzwald and Vosges, Central Europe, *Tectonics* **8,** 1–22.

Fitch, T. J. (1972). Plate convergence, transcurrent faults, and internal deformation adjacent to southeast Asia and the western Pacific, *J. Geophys. Res.* **77,** 4432–4460.

Freymueller, J. T., H. Fletcher, S. Hreinsdóttir, C. F. Larsen, R. Burgmann, E. Calais, and A. Freed (2003). The Denali fault: Crustal deformation before and after the 2002, M_w = 7.9, Denali fault earthquake (abstract), *Eos, Trans. AGU S11B-05*.

Glen, J. M. G., L. Pellerin, J. M. Schmidt, J. A. Sampson, R. Morin, and E. Sanger (2002). Geophysical investigations related to the mineral potential of southcentral Alaska: a summary of results from the Talkeetna Mountains Transect project, presented at Alaska Miners Association Annual Meeting, Anchorage, Alaska.

Grantz, A. (1966). Strike-slip faults in Alaska, *U.S. Geol. Surv. Open-File Rept. 82*, 66.

Gray, D. R., C. J. L. Wilson, and T. J. Barton (1991). Intracrustal detachments and implications for crustal evolution within the Lachlan fold belt, southeastern Australia, *Geology* **19,** 574–577.

Groom, R., and R. Bailey (1989). Decomposition of magnetotelluric impedance tensors in the presence of local three-dimensional galvanic distortion, *J. Geophys. Res.* **94,** 1913–1925.

Harding, T. P. (1985). Seismic characteristics and identification of negative flower structures, positive flower structures, and positive structural inversion, *Am. Assoc. Petrol. Geol. Bull.* **69,** 582–600.

Hickman, R. G., K. W. Sherwood, and C. Craddock (1991). Structural evolution of the early Tertiary Cantwell basin, south central Alaska, *Tectonics* **9,** 1433–1449.

Hillhouse, J. W., and C. S. Gromme (1984). Northward displacement and accretion of Wrangellia: new paleomagnetic evidence from Alaska, *J. Geophys. Res.* **89,** 4461–4467.

Hreinsdóttir, S., J. T. Freymuller, H. J. Fletcher, C. F. Larsen, and R. Burgmann (2003). Coseismic slip distribution of the 2002 M_w 7.9 Denali fault earthquake, Alaska, determined from GPS measurements, *Geophys. Res. Lett.* **30,** 3-1–3-4.

Hyndman, R. D., and M. Shearer (1989). Water in the lower continental crust: modelling magnetotelluric and seismic reflection results, *Geophys. J. Int.* **98,** 343–365.

Iverson, W. P., and S. B. Smithson (1983a). Reprocessed COCORP southern Appalachian reflection data: root zone to Coastal Palin, *Geology* **11,** 422–425.

Iverson, W. P., and S. B. Smithson (1983b). Reprocessing and reinterpretation of COCORP southern Appalachian profiles, *Earth Planet. Sci. Lett.* **62,** 75–90.

Jones, A. G. (1989). MT and reflection: an essential combination, *Geophys. J. R. Astr. Soc.* **89,** 7–18.

Kikuchi, M., and Y. Yamanaka (2002). Source rupture processes of the central Alaska earthquake of Nov. 3, 2002, inferred from teleseismic body waves (+the 10/23 M6.7 event), EIC seismological note 129, Earthquake Research Institute, University of Tokyo, Tokyo. Also available at www.eic.eri.u-tokyo.ac.jp/EIC/EIC_News/021103AL-e.html.

Le Gall, B. (1990). Evidence of an imbricate crustal thrust belt in the southern British Variscides: Contributions of south-western approaches traverse (SWAT) deep sessmic reflection profiling recorded through the English Channel and Celtic Sea, *Tectonics* **9,** 283–302.

Lemiszki, J., and L. D. Brown (1988). Variable crustal structure of strike-slip fault zones as observed on deep seismic reflection profiles, *Geol. Soc. Am. Bull.* **100,** 665–676.

Lu, Z., T. Wright, and C. Wicks (2003). Deformation of the 2002 Denali fault earthquakes, mapped by Radarsat-1 interferometry, *Eos AGU Trans.* **84,** 425–430.

Mathez, E. A., A. G. Duba, C. L. Peach, A. Leger, T. J. Shankland, and G. Plafker (1995). Electrical conductivity and carbon in metamorphic rocks of the Yukon-Tanana terrane, Alaska, *J. Geophys. Res.* **100,** 10,187–10,196.

McClelland, W. C., G. E. Gehrels, S. D. Samson, and P. J. Patchett (1992). Protolith relations of the Gravina belt and YTT in central southeastern Alaska, *J. Geol.* **100,** 107–123.

Miller, T. P. (1994). Geothermal resources of Alaska, in *The Geology of Alaska*, G. Plafker and H. C. Berg (Editors), Geological Society America, Boulder, Colorado, 979–988.

Monger, J. W. H., and H. C. Berg (1987). Lithotectonic terrane map of western Canada and southeastern Alaska, U.S. Geol. Surv. Miscellaneous Field Studies Map MF-1874B, scale 1:2,500,000, 1 sheet.

Morin, R. L., and J. M. G. Glen (2002). Principal facts for 463 gravity stations in the vicinity of Tangle Lakes, east-central Alaska, *U.S. Geol. Surv. Open-File Rept. 02-96*, 21.

Morin, R. L., and J. M. G. Glen (2003). Principal facts for 408 gravity stations in the vicinity of the Talkeetna Mountains, south-central Alaska, *U.S. Geol. Surv. Open-File Rept. 03-27*, 21.

Nokleberg, W. J., N. R. D. Albert, G. C. Bond, L. Herzon, R. T. Miyaoka, W. H. Nelson, D. H. Richter, T. E. Smith, J. H. Stout, W. Yeend, and R. E. Zehner (1982). Geologic map of the southern part of the Mount Hayes quadrangle, Alaska, *U.S. Geol. Surv. Open-File Rept. 82-52*, scale 1:250,000, 1 sheet.

Nokleberg, W. J., J. N. Aleinikoff, and I. M. Lange (1986). Cretaceous deformation and metamorphism in the northeastern Mount Hayes quadrangle, eastern Alaska Range, *U.S. Geol. Surv. Circular 96*, 66–71.

Nokleberg, W. J., H. L. Foster, and J. N. Aleinikoff (1989). Geology of the northern Copper River Basin, eastern Alaska Range, and southern Yukon-Tanana Basin, southern and east-central Alaska, in *Alaskan Geological and Geophysical Transect: 1989 International Geological Congress Guidebook T104*, W. J. Nokleberg and M. A. Fisher (Editors), American Geophysical Union, Washington, D.C., 34–63.

Nokleberg, W. J., D. L. Jones, and N. J. Silberling (1985). Origin and tectonic evolution of the Maclaren and Wrangellia terranes, eastern Alaska Range, Alaska, *Geol. Soc. Am. Bull.* **96,** 1251–1270.

Nokleberg, W. J., G. Plafker, and F. H. Wilson (1994). Geology of south-central Alaska, in *The Geology of Alaska*, G. Plafker and H. C. Berg (Editors), Geological Society of America, Boulder, Colorado, 311–366.

Panuska, B. C. (1990). An overlooked, world class Triassic flood basalt event, *Geol. Soc. Am. Abs. Prog.* **22,** no. 7, 168,

Park, S. K., and B. Wernicke (2003). Electrical conductivity images of Quaternary faults and Tertiary detachments in the California Basin and Range, *Tectonics* **22,** 4-1–4-17.

Pellerin, L., and G. W. Hohmann (1990). Transient electromagnetic inversion: a remedy for magnetotelluric static shifts, *Geophysics* **55,** 1242–1250.

Plafker, G., L. M. Gilpin, and J. C. Lahr (1994). Neotectonic map of Alaska, in *The Geology of Alaska*, G. Plafker and H. C. Berg (Editors), Geological Society of America, Boulder, Colorado, 1 sheet.

Plafker, G., W. J. Nokleberg, and J. S. Lull (1989). Bedrock geology and tectonic evolution of the Wrangellia, Peninsular, and Chugach terranes along the Trans-Alaskan Crustal Transect in the northern Chugach Mountains and southern Copper River Basin, Alaska, *J. Geophys. Res.* **94,** 4255–4295.

Pratt, T. L., E. C. Hauser, T. M. Hearn, and T. J. Reston (1991). Reflection polarity of the midcrustal Surrency bright spot beneath southeastern Georgia: Testing the fluid hypothesis, *J. Geophys. Res.* **96,** 10,145–10,158.

Ratchkovski, N. A., R. A. Hansen, J. C. Stachnik, T. Cox, O. Fox, L. Rao, E. Clark, M. Lafevers, S. Estes, J. B. MacCormack, and T. Williams (2003). Aftershock sequence of the M_w 7.9 Denali fault, Alaska, earthquake of 3 November, 2002 from regional seismic network data, *Seism. Res. Lett.* **74,** 743–752.

Richter, D. H. (1976). Geologic map of the Nabesna quadrangle, Alaska, U.S. Geol. Surv. Miscellaneous Geological Investigations Series Map I-932, scale 1:250,000, 1 sheet.

Richter, D. H., and D. L. Jones, (1973). Structure and stratigraphy of the eastern Alaska Range, Alaska, in *Arctic Geology*, Memoir 19, Am. Assoc. Petrol. Geol., 408–420.

Richter, D. H., and N. A. Matson (1971). Quaternary faulting in the eastern Alaska Range, *Geol. Soc. Am. Bull.* **82,** 1529–1540.

Ridgway, K. D., J. M. Trop, W. J. Nokleberg, C. M. Davidson, and K. R. Eastham (2002). Mesozoic and Cenozoic tectonics of the eastern and central Alaska Range; progressive basin development and deformation in a suture zone, *Geol. Soc. Am. Bull.* **114,** 1480–1504.

Rodi, W., and R. L. Mackie (2001). Nonlinear conjugate gradients algorithm for 2D magnetotelluric inversion, *Geophysics* **66,** 174–187.

Rubin, C. M., and J. B. Saleeby (1991). The Gravina sequence: Remnants of a mid-Mesozoic oceanic arc in southern southeast Alaska, *J. Geophys. Res.* **96,** 14,551–14,568.

Saltus, R. W., and G. C. Simmons (1997). Composite and merged aeromagnetic data for Alaska: a website for distribution of gridded data and plot files, *U.S. Geological Survey Open-File Rept. 97-520*. http://pubs.usgs.gov/of/1997/ofr-97-0520/alaskamag.html.

Sanger, E. A., and J. M. G. Glen (2003). Density and magnetic susceptibility values for rocks in the Talkeetna Mountains and adjacent region, south-central Alaska, *U.S. Geol. Surv. Open-File Rept. 03-268*, 20.

Sibson, R. H. (1982). Fault zone models, heat flow, and the depth distribution of earthquakes in the continental crust of the United States, *Bull. Seism. Soc. Am.* **72,** 151–163.

Smith, J. T., and J. R. Booker (1991). Rapid inversion of two- and three-dimensional magnetotelluric data, *J. Geophys. Res.* **96,** 3905–3922.

Smith, T. E. (1981). Geology of the Clearwater Mountains, south-central Alaska, Alaska Division of Geological and Geophysical Surveys Geologic Report 60, 72 pp., 1 sheet, scale 1:63,360.

Smithson, S. B., R. A. Johnson, and C. A. Hurich (1986). Crustal reflections and crustal structure, in *Reflection Seismology: A Global Perspective*, M. Barazangi and L. Brown (Editors), Geodynamic Series Vol. **14,** American Geophysical Union, Washington, D.C., 21–32.

Smithson, S. B., F. Wenzel, Y. V. Ganchin, and I. B. Morozov (2000). Seismic results at Kola and KTB deep scientific boreholes: velocities, reflections, fluids, and crustal composition, *Tectonophysics* **329,** 301–317.

Sontag, L. J., and B. C. Panuska (1990). Paleomagnetic data from Triassic intrusives in the Wrangell Mountains, Alaska; implications for the age of magnetization of Paleozoic rocks, *The Compass* **67,** 263–268.

Stanley, W. D. (1986). Magnetotelluric study of a compressed flysch system in the Healy quadrangle, *U.S. Geol. Surv. Circular 928*, 46–50.

Stanley, W. D. (1989). Comparison of geoelectrical/tectonic models for suture zones in the western U.S. and eastern Europe: Are black shales a possible source of high conductivities?, *Phys. Earth Planet. Interiors* **53,** 228–238.

Stanley, W. D., V. F. Labson, W. J. Nokleberg, B. Csejtey, and M. A. Fisher (1990). The Denali fault system and Alaska Range of Alaska: Evidence for underplated Mesozoic flysch from MT surveys, *Geol. Soc. Am. Bull.* **102,** 160–173.

Stone, D. B., J. C. Roe, and B. C. Panuska (1991). Paleomagnetic latitude variations in time and space along the Trans Alaska Crustal Transect, *Geol. Soc. Am. Abs. Prog.* **23,** no. 2, 101.

Stout, J. H. (1976). Geology of the Eureka Creek area, east-central Alaska Range, Alaska Division of Geological and Geophysical Surveys Geologic Reptort 46, 32.

Stout, J. H., J. B. Brady, F. R. Weber, and R. A. Page (1973). Evidence for Quaternary movement on the McKinley strand of the Denali fault in the Delta River area, Alaska, *Geol. Soc. Am. Bull.* **84,** 939–947.

Trop, J. M., K. D. Ridgway, J. D. Manuszak, and P. Layer (2002). Mesozoic sedimentary-basin development on the allochthonous Wrangellia composite terrane, Wrangell Mountains basin, Alaska: a long-term record of terrane migration and arc construction, *Geol. Soc. Am. Bull.* **114,** 693–717.

Turner, D. L., and T. E. Smith (1974). Geochronology and generalized geology of the central Alaska Range, Clearwater Mountains and northern Talkeetna Mountains, Alaska Div. Geol. Geophys. Surv. Geol. Open-File Rept. AOF-72, 10.

Unsworth, M. J., P. Bedrosian, M. Eisel, G. Egbert, and W. Siripunvaraport (2000). Along strike variations in the electrical structure of the San Andreas fault at Parkfield, California, *Geophys. Res. Lett.* **27,** 3021–3024.

Unsworth, M. J., G. Egbert, and J. Booker (1999). High-resolution electromagnetic imaging of the San Andreas fault in central California, *J. Geophys. Res.* **104,** 1131–1150.

Unsworth, M. J., P. E. Malin, G. D. Egbert, and J. R. Booker (1997). Internal structure of the San Andreas fault at Parkfield, California, *Geology* **25,** 359–362.

Vozoff, K., (1991). The magnetotelluric method, in *Electromagnetic Methods in Applied Geophysics*, M. N. Naibighian (Editor), Society of Exploration Geophysicists, Tulsa, Oklahoma, 641–711.

Wahrhaftig, C., D. L. Turner, F. R. Weber, and T. E. Smith (1975). Nature and timing of movement on the Hines Creek strand of the Denali fault system, Alaska, *Geology* **3,** 463–466.

Waldhauser, F., and W. L. Ellsworth (2000). A double-difference location algorithm: Method and application to the northern Hayward fault, California, *Bull. Seism. Soc. Am.* **90,** 1353–1368.

Wallace, W. K., C. L. Hanks, and J. F. Rogers (1989). The southern Kahiltna terrane: Implications for the tectonic evolution of southwestern Alaska, *Geol. Soc. Am. Bull.* **101,** 1389–1407.

Wannamaker, P. E. (1986). Electrical conductivity of water-undersaturated crustal melting, *J. Geophys. Res.* **91,** 6321–6327.

Wannamaker, P. E., G. W. Hohmann, and S. H. Ward (1984). Magnetotelluric responses of three-dimensional bodies in layered earths, *Geophysics* **49,** 1517–1533.

Wannamaker, P. E., G. R. Jiracek, J. A. Stodt, T. G. Caldwell, V. M. Gonzalez, J. D. McKnight, and A. D. Porter (2002). Fluid generation and pathways beneath an active compressional orogen, the New Zealand Southern Alps, inferred from magnetotelluric data, *J. Geophys. Res.* **107,** ETG 6-1–ETG 6-20.

Wannamaker, P. E., J. A. Stodt, and L. Rijo (1987). A stable finite element solution for two-dimensional magnetotelluric modeling, *Geophys. J. R. Astr. Soc.* **88,** 277–296.

Williams, C. F., L. A. Beyer, F. V. Grubb, and S. P. Galanis (2001). Heat flow and seismotectonics of the western Transverse Ranges, *Geol. Soc. Am. Abs. Prog.* **33,** 63.

Wright, T. J., L. Zhong, and C. Wicks (2003). Source model for the Mw 6.7, 23 October 2002, Nenana Mountain Earthquake (Alaska) from InSAR, *Geophy. Res. Lett.* **30,** SDE 12-1–SDE 12-4.

Appendix

A general philosophy about modeling geophysical data holds that statistically significant features can be retrieved from inverse models and that a large number of inverse models should be produced; only those features that appear in all of them should be deemed to be significant and not merely artifacts of the inversion scheme (Backus and Gilbert, 1967). Following this philosophy, we produced 35 inverse models of MT data, using the Rapid Relaxation Inversion (RRI) (Smith and Booker, 1991), the 2D Occam's inversion (de Groot-Hedlin and Constable, 1990) and the conjugate gradient (CG) method (Rodi and Mackie, 2001). Data for both the TE and TM modes and the TM mode alone were inverted, using different starting models. The Earth's surface was approximated by digitized topography or a flat surface. In addition, various rotations of the impedance matrix with respect to the principle axis were examined, and different mesh discretizations were used. The results fell into three categories: significantly similar models with the TM mode alone and an root-mean-square (rms) fit of approximately 3, similar models from both the TM and TE modes with rms fit of about 12 in which the poor fit was due to the TE mode at all frequencies for station 735 and for station 740 for frequencies down to 0.01 Hz, or the solution did not converge.

In a 2D environment the diagonal terms of the impedance matrix, which relates the magnetic to the electric field data, are zero, and the TM and TE modes are contained in the off-diagonal terms. The impedance matrix reduces to a scalar quantity for a layered or 1D earth, and this matrix is full in a 3D environment. Electrical strike can be estimated, with a 90° ambiguity, through a rotation of the impedance matrix to minimize the diagonal terms. If the matrix is rotated at each frequency, the strike direction and corresponding mode determination varies with frequency and depth, possibly making the concept of strike nebulous. Acquiring the data along a profile perpendicular to strike is preferable, but this is not always a viable option. In this study the Richardson Highway provided easy logistical access; however, the highway was there because of a pass through the mountains that corresponds to complex geology. Hence the issue of strike and mode determination is of particular importance.

Impedance strike estimated at three frequencies is shown in Figure A1. The profile line is not perpendicular to strike, and the strike direction is somewhat inconsistent from site to site and frequency to frequency. Variations in estimated electrical strike can arise from splays off the main fault and 3D structures, making mode determination problematic. Also near-surface inhomogeneities can distort the impedance strike at depth (Groom and Bailey, 1989). Given the regional strike, the *xy* mode is closest to the TM mode. The data can also be rotated to the principle axes at each frequency and the resulting TM dataset modeled. If the strike direction varies at each frequency, the latter technique would mix modes from frequency to frequency and the physical significance of strike would be lost.

Two 2D models, which can be considered end members, are presented for investigation: the TM mode produced from rotation to principle axis (Fig. 8) and for the acquired *xy* mode fixed as the TM mode (Fig. A2). The major features of R1 to R4 are present in both models, but some departures exist that should be considered in the interpretation. Both models fit the MT data reasonably well with an rms of about 3. However, the preferred model, presented previously, is simpler, more consistent with the other geophysical data, and more geologically reasonable.

The alternative model is computed from the fixed *xy* mode (Fig. A2). The corresponding apparent resistivity and phase pseudosections for observed data and model response, or calculated data (Fig. A3), show the model fit. The primary differences are the conductor at depth that breaks up unit R1 under sites 735 and 755, which is not present in the first

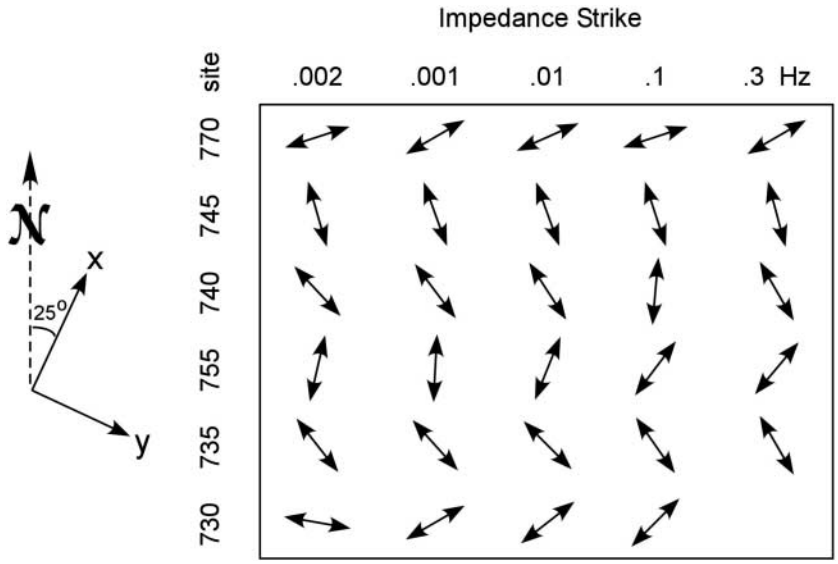

Figure A1. Impedance strike determination for 1, 0.1, and 0.01 Hz.

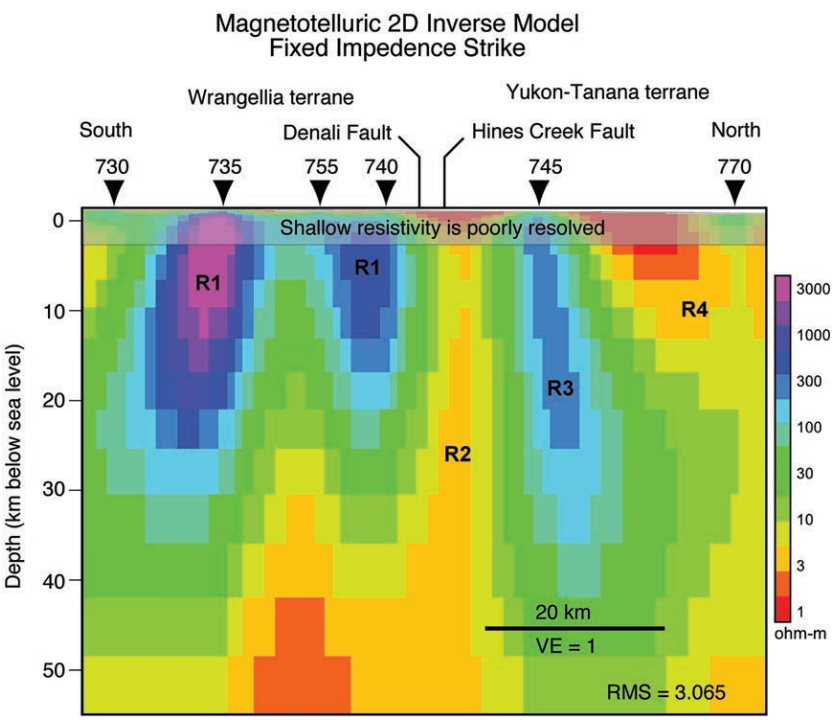

Figure A2. Two-dimensional inverse MT model using the TM mode from the principle axis rotation and inversion using the conjugate gradient method. The mapped geology is noted above the model. The four units (R1–R4) are discussed in the text.

model, and the model is generally more conductive, but not enough to change significantly the major points in the interpretation. As with the first model, the fit is poorest south of the Denali fault in the area mapped as Wrangellia.

Trial-and-error forward modeling can also be used to ascertain the sensitivity of a model to the data. By using the 2D finite-element code of Wannamaker *et al.* (1987) resistivity values can be changed and the forward response computed. Because this is a pure 2D forward model, no off-line structures can be modeled. For the presented models, forward modeling shows that structure in the upper part of the section is insensitive to the acquired data. Because the southern portion of the section is quite resistive with values on the order of a 1000 Ω m and the northern portion is rather conductive with values ranging in tens of ohms m, this zone of insensitivity ranges from roughly 15 to 2 km, respectively. The presence of the large features at depth denoted by R1 to R4 is supported with forward modeling. The value of R1 varied from 3000 to 10,000 Ω·m, R2 from 5 to 20 Ω·m, R3 from 200 to 500 Ω·m, and R4 from 10 to 20 Ω·m.

Error is introduced into the model because of the assumption of a 2D earth. The two models presented help to increase confidence that the structures R1 through R4 are indeed present and both models suffer from similar 3D ef-

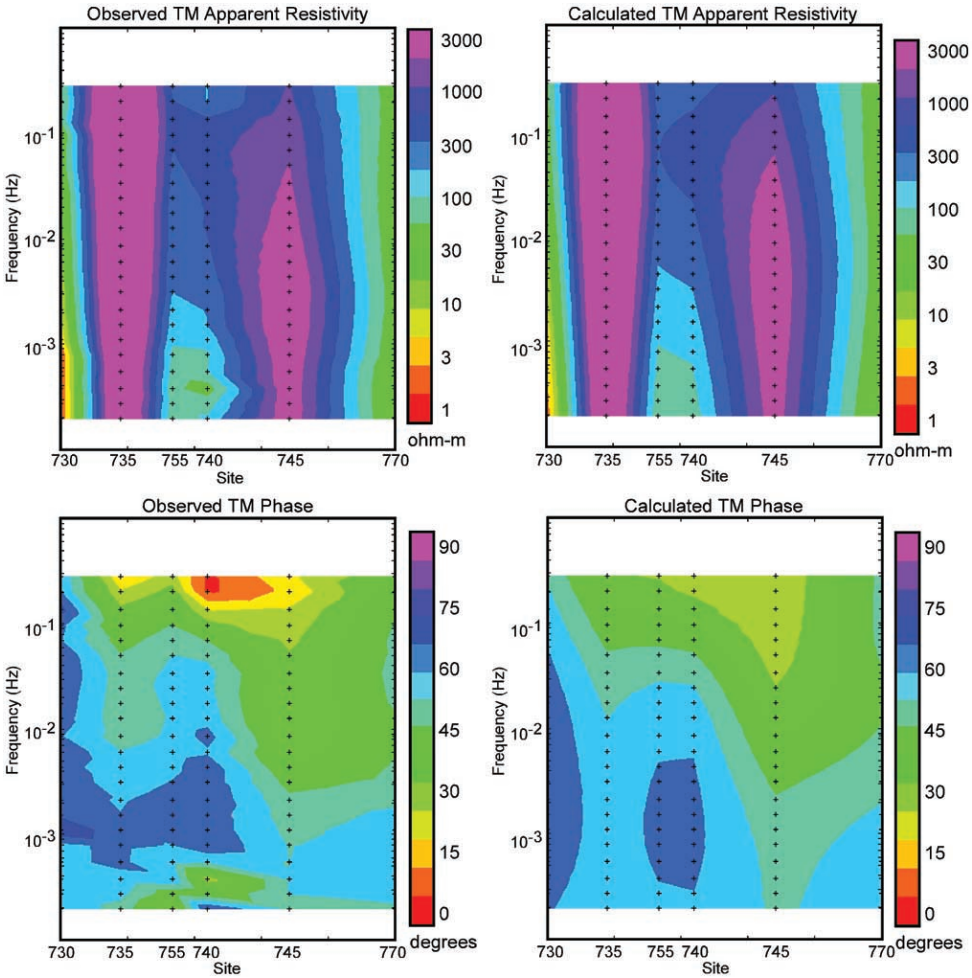

Figure A3. The observed (left) and calculated (right) apparent resistivity (top) and phase (bottom) of the 2D model of Figure A2 presented in pseudosection format to illustrate how well the observed and calculated values compare.

fects. The two stations that were most difficult to fit were 735 and 740, on each side of body R1. When both modes are modeled the TE mode at site 735 is depressed, but parallel to the TM, indicating inhomogeneities in the section above the zone of investigation. Distortions in the electric field measurements by relatively near-surface inhomogeneities are known as static shifts (Pellerin and Hohmann, 1990) and are best corrected using an independent dataset, which is not available for this survey. Ad hoc shifting of curves to account for an apparent shift resulted in a solution that did not converge. Station 740 is just south of the Denali fault where the mapped geology is rather complex. The TE mode fits the data very poorly from about 0.1 to 0.01 Hz, and the TM mode fit is poor above 0.1 Hz.

U.S. Geological Survey
345 Middlefield Rd.
Menlo Park, California 94025
mfisher@usgs.gov
(M.A.F., W.J.N., J.M.G.G.)

Geophysical Institute
University of Alaska
P.O. Box 757320
Fairbanks, Alaska 99775
(N.A.R.)

Green Engineering, Inc.
2215 Curtis St.
Berkeley, California 94702
(L.P.)

Manuscript received 30 January 2004.